Princeton Plasma Physics Laboratory

PPPL- 4528

PPPL- 4528

Transient Enhancement ('Spike-on-Tail') Observed on Neutral-Beam-Injected Energetic Ion Spectra Using the E||B Neutral Particle Analyzer in the National Spherical Torus Experiment

S. S. Medley, N. N. Gorelenkov, R. E. Bell, E. D. Fredrickson, S. P. Gerhardt, B. P. LeBlanc, M. Podestà, A. L. Roquemore, and the NSTX Team

June, 2010

PPPL
PRINCETON PLASMA PHYSICS LABORATORY

Prepared for the U.S. Department of Energy under Contract DE-AC02-09CH11466.

Princeton Plasma Physics Laboratory
Report Disclaimers

Full Legal Disclaimer

Trademark Disclaimer

PPPL Report Availability

Princeton Plasma Physics Laboratory:

http://www.pppl.gov/techreports.cfm

Office of Scientific and Technical Information (OSTI):

http://www.osti.gov/bridge

Related Links:

U.S. Department of Energy

Office of Scientific and Technical Information

Fusion Links

Transient Enhancement ('Spike-on-Tail') Observed on Neutral-Beam-Injected Energetic Ion Spectra Using the EIIB Neutral Particle Analyzer in the National Spherical Torus Experiment

S. S. Medley, N. N. Gorelenkov, R. E. Bell, E. D. Fredrickson, S. P. Gerhardt,
B. P. LeBlanc, M. Podestà, A. L. Roquemore, and the NSTX Team

Princeton Plasma Physics Laboratory, Princeton, New Jersey, 08543, USA

Email: *medley@pppl.gov*

Abstract

An increase of up to four-fold in the EIIB Neutral Particle Analyzer (NPA) charge exchange neutral flux localized at the Neutral Beam (NB) injection full energy is observed in the National Spherical Torus Experiment (NSTX). Termed the High-Energy Feature (HEF), it appears on the NB-injected energetic ion spectrum only in discharges where tearing or kink-type modes ($f < 10$ kHz) are absent, TAE activity ($f \sim 10$-150 kHz) is weak ($\delta B_{rms} < 75$ mGauss) and CAE/GAE activity ($f \sim 400 - 1200$ kHz) is robust. The feature exhibits a growth time of ~ 20 - 80 ms and occasionally develops a slowing down distribution that continues to evolve over periods of 100's of milliseconds, a time scale long compared with the typical ~ 10's ms equilibration time of the NB injected particles. The HEF is observed only in H-mode (not L-mode) discharges with injected NB power of 4 MW or greater and in the field pitch range $v_{||}/v \sim 0.7 - 0.9$; i.e. only for passing (never trapped) energetic ions. The HEF is suppressed by vessel conditioning using lithium deposition at rates ~ 100 mg/shot, a level sufficient to suppress ELM activity. Increases of ~ 10 - 30 % in the measured neutron yield and total stored energy are observed to coincide with the feature along with broadening of measured Te(r), Ti(r) and $n_e(r)$ profiles. However, TRANSP analysis shows that such increases are driven by plasma profile changes and not the HEF phenomenon itself. Though a definitive mechanism has yet to be developed, the HEF appears to be caused by a form of TAE/CAE wave-particle interaction that distorts of the NB fast ion distribution in phase space.

1.0 Introduction

The National Spherical Torus Experiment (NSTX) [1] is a midsize low aspect ratio fusion research facility with auxiliary heating from Neutral Beam Injection (NBI) and High Harmonic Fast Wave (HHFW) launch. Typical NSTX parameters are major radius R_0 = 0.85 - 0.9 m, minor radius a = 0.67 m resulting in an aspect ratio of $A = R_o/a \sim 1.3$, plasma current I_p = 0.3 - 1.5 MA and toroidal field B_T = 0.3 - 0.6 T. Three co-directed deuterium neutral beam sources have injected power up to P_{NB} = 7 MW at full neutral energies up to E_b = 100 keV. HHFW heating at 30 MHz has delivered up to $P_{RF} \sim 6$ MW to deuterium and helium plasmas.

Determining the attractiveness of the spherical torus concept [2] in the areas of high-β stability, confinement, non-inductive current drive and divertor physics for pulse lengths much longer than the energy confinement time is the mission of the NSTX device. The performance milestones that were achieved to date in NSTX have been reported elsewhere [3-5]. H-modes triggered by NBI heating are routinely obtained in NSTX and have become a standard operational scenario [6]. L-H transitions triggered by NBI heating have been obtained over a wide parameter range in $I_p \leq 1.2$ MA, $B_T \leq 5.5$ kGauss, and $n_e \leq 8 \times 10^{13}$ cm^{-3} in either lower-single-null or double-null diverted discharges with elongation $\kappa \leq 2.6$, triangularity $\delta \leq 0.85$ and plasma pulse length exceeding 1.5 s.

The physics of plasmas that contain large populations of super-Alfvénic energetic particles is an important outstanding issue for burning plasma experiments, such as ITER. NSTX is particularly well suited to investigate fast-ion driven instabilities and their influence on fast particle confinement. A wide variety of fast ion driven instabilities are excited during high-power NBI in NSTX. TAEs [7] and other Alfvén eigenmodes [8] are destabilized when the fast-ion velocity v_b is larger than the Alfvén speed v_A. The modes can be divided into three categories; chirping Energetic Particle Modes (EPM) in the frequency range 0 – 120 kHz, the Toroidal Alfvén Eigenmodes (TAE) with a frequency range of 50 – 200 kHz and the Global and Compressional Alfvén Eigenmodes (GAE and CAE, respectively) between 300 kHz and the ion cyclotron frequency. Some of the higher frequency modes exhibit a frequency splitting characteristic of what would be expected

from “hole-clump” theory [9]. The TAEs can appear either as saturated modes or as bursting modes and the bursting TAEs observed in NSTX [10] can cause significant fast ion losses.

In addition to Alfvénic modes, energetic ion redistribution associated with low frequency tearing or internal kink-type magnetohydromagnetic (MHD) activity has been observed in many fusion experiments, for example, NSTX [11,12] and ASDEX-U [13,14]. Outward redistribution of the core-peaked energetic beam ions due to Alfvénic modes can modify the NBI-driven current profile and hence the core q-profile, as also reported in DIII-D [15,16].

If MHD-induced energetic ion redistribution is sufficiently severe then ion loss to the NSTX first-wall structures can occur in addition to bad-orbit driven prompt loss to the walls. The prompt loss of neutral beam ions from NSTX is expected to be between 12% and 42% of the total beam power [17]. Such losses are diagnosed either from temperature measurements of ion deposition on first wall structures or by Faraday cup probes [18] which detect ions on loss orbits. Also, orbit excursions beyond the separatrix can result in a depletion of the energetic ion population due to charge exchange losses and a potentially create a ‘bump-on-tail’ in the energetic ion distribution [19].

Resonant interaction of high-energy particles with magnetic perturbations in toroidal devices can produce large-scale modification of the particle distribution, sometimes leading to particle loss. Spherical tokamaks, including NSTX [20 – 23], START [24] and MAST [25, 26], are particularly susceptible to fast ion driven instabilities due primarily to their relatively low toroidal field but also in some instances due to the direct effect of the low aspect ratio. The loss of energetic ions on NSTX has been confirmed by direct measurement of ion losses with a scintillator Fast-Loss Ion Probe (sFLIP) [27].

In quiescent or MHD benign NSTX discharges, NPA measurements of the energetic beam ion distribution are consistent with classical behavior [28]. However, the appearance of MHD activity can have a pronounced effect on ‘energetic’ ($E \sim 10 – 100$ keV) ion populations in NSTX. A rich variety of energetic deuterium ion behavior resulting from MHD activity has been observed in NSTX [11, 29-31] using the ElIB neutral particle analyzer diagnostic.

2.0 Diagnostics for Investigation of Wave-Particle Effects on Energetic Ions in NSTX

On NSTX, the amplitude and structure of Alfvén modes are measured using a suite of diagnostics, including Mirnov magnetic coils, Ultra Soft X-Ray (USXR), and reflectometry diagnostics. The neutron production in NSTX is predominantly from beam-target reactions and thus is a robust measure of the energetic ion behavior. Neutron data along with NPA and sFLIP diagnostics are used to assess fast-ion redistribution or loss due to MHD-induced effects. Diagnostics for spatial localization of MHD activity in NSTX H-mode discharges are limited with USXR arrays being one of the most effective.

Energetic ion distributions are usually measured using charge exchange neutral particle diagnostics [32]. The NPA on NSTX [33] utilizes a PPPL-designed ElIB spectrometer [34] which measures the mass-resolved energy spectra of H and D neutrals simultaneously with a time resolution of ~1 ms set by signal-to-noise levels. The calibrated energy range is E = 0.5 – 150 keV and the energy resolution varies over a range of $\Delta E/E$ = 3 - 7% from high to low energy.

As shown in Fig. 1, the NPA views across the co-injection paths of the three NBI sources on NSTX that inject at major radii R_{NB} = 69.4 cm (source A), R_{NB} = 59.2 cm (source B) and R_{NB} = 48.7 cm (source C) and can be scanned horizontally over a wide range of tangency radii (as well as vertically) on a shot-to-shot basis. Spatial localization of the NPA flux arises from the intersection of the diagnostic sightline with the NBI sources as illustrated in Fig. 2. The inset in panel (a) shows the pitch angle variation along the NPA sightline. The spatial localization weakens at smaller NPA tangency radii, R_{tan}, due to attenuation of the beam neutral density with increasing penetration distance. Panel (b) shows the spatial localization of the NPA measurement in terms of the major radius of the intersection of the NPA sightline with the NB axis. For vertical scanning, the maximum accessible elevation minor radius depends on the choice of horizontal tangency radius (panel (d)). As shown in panel (c), the localization of the NPA measurements in space and pitch angle discussed above is strongest near the NBI full energy, but remains substantial over the entire slowing down distribution.

3.0 Representative High-Energy Features on Energetic Ion Spectra in NSTX

A transient increase in the NPA charge exchange flux that is localized at the NB full energy has been observed on NSTX that will be referred to as the "High-Energy Feature" or HEF. This feature has been observed over an extensive range of discharges during the 2008-09 NSTX campaigns. A subset of the HEF database is shown in Table I. The HEF is observed only at the NB full injection energy: i.e. never at the NB fractional energies. The HEF exhibits rise-times of ~ 20 – 80 ms and durations up to 100's of milliseconds and multiple HEFs can occur during a single discharge. Discharge conditions that appear to be simultaneously necessary (but not necessarily sufficient) for HEFs to occur are: H-modes, $P_b \geq 4$ MW, no n=1 kink-like modes and reduced TAE activity.

Excursions in S_n and W_T are frequently observed during HEFs, but appear not to be caused by the energetic ions associated with the HEF event itself as demonstrated in Section 5.0: TRANSP Code Analysis.

The HEF moves to different MCP anodes when the NPA E||B fields are varied: i.e. it is not an instrumental effect. For the cases examined, the magnitude of the slowed-down distribution during the high-E feature is the same as before the high-E feature: i.e. the feature is not due to some increased loss in the slowing down distribution. Ions are not accelerated above NB injection energy. The HEF ions transit the core region intersecting the NB footprint. This is verified by examining a programmed NBI power notch (e.g. 127236, not shown) that causes prompt reduction of the HEF signal (on the timescale of primary neutral drop). However, the notch drives $P_b < 4$ MW thus violating a condition needed for occurrence of the HEF and possibly complicating the situation. HEF recovery following notch is "gradual" as is always the case at the initial appearance: i.e. the HEF always has a growth time. Evolution of a slowing-down distribution below the HEF is only rarely observed, and then the evolution is very slow (100's ms) compared with normal beam slowing down times (10's ms). HEFs have been observed for mid-plane NPA sightlines with: $R_{tan} \sim 55 – 90$ cm, $v_{||}/v \sim 0.7 – 0.9$. No systematic horizontal scans are available.

Table I: Abridged Overview of HEF Characteristics

Shot	Δt(ms)	B_T	I_p	R_T	δB_{TAE}	δB_{CAE}	ΔS_n(%)	ΔW_T(%)	Comments
127236	450-670	4.5	0.9	71	24	0.75	Δ Pb	Δ Pb	Tandem HEFs track δB_{TAE} structure
127256	430-540	4.5	0.9	65	14	~0.5	0	5	sFLIP correlates with HEF
128820	380-520	4.5	0.9	65	24	1.6	Δ Pb	Δ Pb	HEF for 1st NB blip
128895	320-920	4.5	1.1	70	20	0.8	18	15	Classic Tandem HEFs
132483	470-720	4.5	0.9	70	34	~1.5	22	ND	Choppy HEF, fiducial w/ SPAs, S_n odd
132484	520-720	4.5	0.9	70	33	1.0	39	26	Choppy HEF, fiducial w/o SPA, S_n ramp
132541	420-760	4.5	1.0	70	38	1.1	40	35	Dual HEF w/2nd bursting, $S_n$ramp
132542	420-700	4.5	1.0	70	37	1.0	32	26	Choppy HEFs w/later bursting, S_n ramp
132546	400-800	4.5	0.9	70	24	~1.7	20	36	Strong, tandem HEFs, delayed S_n step
132550	440-720	4.5	1.0	70	14	~1.4	0	15	HEFs@70/90 1ST LITER@200 mg/shot
132552	450-760	4.5	1.0	70	15	~1.5	10	23	HEFs@70/90keV
132787	540-840	4.5	0.9	70	43	~1.7	37	18	Strong HEF with later bursting, S_n step
132790	500-620	4.5	0.9	70	28	~1.4	11	7	A,C @ 90 keV, P_b = 4 MW
132800	480-600	4.5	1.0	70	24	~1.5	33	16	Classic "brief" HEF, S_n step
132806	420-900	4.5	1.0	70	21	1.1	20	20	Weak HEF with later bursting, S_n ramp
132809	420-1120	4.5	1.0	70	20	~1.6	20	26	Weak HEF with later bursting, S_n ramp
132928	200-600	4.5	0.8	70	5	~1.5	x	x	Persistent HEF, odd δB_{TAE},S_n ramp
133025	560-920	4.5	0.9	70	36	~1.6	16	21	Choppy HEF, irregular S_n evolution
133346	600-1200	4.5	0.9	70	16	1.0	0	0	NPA chop modulates HEF
133593	500-800	4.5	0.9	70	40	1.2	25	ND	Modest, choppy HEF
133600	500-650	4.5	0.9	70	36	1.4	12	ND	Strong, clean HEF
133721	450-700	4.5	0.9	70	35	1.6	20	30	Choppy HEF: none on ssNPA.
133723	470-600	4.5	0.9	70	32	1.5	18	15	Strong, clean HEF: none on ssNPA.
133737	620-1200	4.5	0.9	70	~15	1.5	0	33	Strong HEFs: large S_n/S_{npa} chop
133738	620-920	4.5	0.9	70	14	1.3	23	31	Strong, dual HEFs: large S_n/S_{npa} chop
133803	500-1000	4.5	0.9	63	15	1.7	6	10	Long, weak, choppy HEF
133913	620-1060	4.5	0.9	70	31	1.3	0	0	Strong HEF, later bursting: S_n/S_{npa} chop
133914	440-1080	4.5	1.0	70	23	1.2	23	24	Strong HEF, later bursting: S_n/S_{npa} chop
134169	570-1280	4.5	0.9	70	24	1.3	0	22	Long, weak, choppy HEF
134269	440-770	5.0	1.2	70	11	1.0	29	30	Long, modest, choppy HEF: P_b = 4 MW
134764	540-960	4.5	0.9	70	26	1.0	0	0	Chop obscures HEF, modulates S_n
134765	500-1200	4.5	0.9	70	16	1.1	0	0	Large chop obscures HEF, CAE Mod'n
134783	300-650	5.5	1.1	70	50	1.0	0	13	Very weak HEF. High δB_{TAE}
135153	410-800	4.5	0.8	70	21	1.4	49	47	Classic HEF: P_b = 4 MW, gap 7.5 cm
135155	470-650	4.5	0.8	70	33	1.1	17	16	Clean HEFs @65/90 keV, choppy S_n
135156	400-1000	4.5	0.8	70	60	1.0	x	?	Persistent HEF @65 keV, S_n odd δB_{TAE}
135172	400-720	4.5	0.8	90	42	1.4	13	17	Huge, clean HEF @65 keV, choppy S_n
135174	400-1000	4.5	0.8	70	27/180	~2.0	0	15	Huge, clean, tandem HEFs @65/90 keV
135175	400-1000	4.5	0.8	70	28/140	~1.7	12	30	Huge, overlapping HEFs @65/90 keV

3.1 Non-HEF Reference Discharge: SN135047

In the subsections below, examples are presented of HEFs that are classified according to selected dominant characteristics. First, however, data for a discharge devoid of the HEF event will be presented to provide a reference for comparison with the representative discharges that do exhibit HEF events.

Figure 3 shows a typical NPA deuterium fast-ion spectrum characterized by energetic ion depletion in the range $E_b/2 < E \leq E_b$ that is driven by a combination of attenuation of injected NB neutrals and emerging charge exchange flux caused by rising electron density as well as potential MHD-induced energetic ion redistribution or loss [11]. The upper plot shows the NPA 3D energetic ion spectrum and the lower plot gives spectrum line-outs at t = 200, 350, 450 and 900 ms showing the progressive depletion of the spectra.

Figure 4 shows Mirnov spectrograms for the CAE/GAE modes in the frequency range, f = 400- 1200 kHz in panel (a) and for the NTM/TAE modes frequency in the range $f \leq 140$ kHz in panel (b) with injected NB power, P_b(MW), the NPA signal at E_b = 90 keV, S_{npa}(au), and total neutron yield, S_n(au) shown in panel (c).

Figure 5 shows a collection of discharge data that is relevant to this study. Panel (a) gives waveforms for plasma current, I_p(MA), injected NB power, P_b(MW) and line-averaged electron density, $n_e(x10^{13}\ cm^{-3})$, provided the Multi Point Thomson Scattering (MPTS) diagnostic. Panel (b) identifies MHD toroidal modes for n = 1 – 8 obtained by FFT analysis of the Mirnov spectrograms shown in Fig. 4a and panel (c) is the corresponding analysis for n = 1 – 4 shown in Fig. 4(b). Panel (d) shows the contour plot of the NPA flux versus energy and time corresponding to the 3D spectrum shown in Fig. 3. Panel (e) gives measured waveforms for neutron yield, $S_n(x10^{13}s^{-1})$, total stored energy, W_T(kJ) and lower divertor D_α emission (au).

Figure 6 provides contour plots of MPTS measurements of electron temperature (a) and density (c) and Charge Exchange Recombination Spectroscopy (CHERS) measurements of deuterium ion temperature (b), toroidal rotation velocity (d) and carbon impurity Z_{eff} (e).

The figure formats used in this section will also be used in Sec. 3.2 – 3.4 and will not be re-described in those sections.

3.2 'Transient' High-Energy Feature: SN132800

A 'transient' HEF is characterized by being a single event with a duration in the range of t ~ 100 – 300 ms. A classic case in shown in the upper plot of Fig. 7 where the

HEF occurs in the interval t = 480 – 600 ms identified by the blue circle in on the NPA 3D energetic ion spectrum. The lower plot shows spectra line-outs at t = 400, 500, and 550 ms. From this figure, it is evident that the HEF occurs at the NB full injection energy, E_b = 90 keV, and not at the NB fractional energies, $E_b/2$ = 45 keV and $E_b/3$ = 30 keV. Also notable is the absence of any slowing-down distribution evolving from the HEF energy. The spectrum was obtained for a NPA tangency radius of R_{tan} = 70 cm that localizes the measurement (see Fig. 2) to the intersection with the NB footprint at a major radius of R_{int} ~ 85 cm. The HEF is strikingly evident by the transiently enhanced NPA flux at E_b = 90 keV seen in the black curve in panel (c) of Fig. 8 demarked by the vertical blue bar. This figure also illustrates MHD behavior that is commonly observed with HEF events. Firstly, the HEF occurrence requires that f < 10 kHz, n = 1 tearing or kink-type MHD is absent and TAE activity is minimal as seen in panel (b). Secondly, as seen in panel (a) the CAE/GAE activity can be robust and appears to be unaffected (i.e. is not modulated) by the HEF. Thirdly, reappearance n = 1 modes, strong TAE activity or bursting MHD (e.g. EPMs or TAE 'avalanches') terminates the HEF as seen in this case at t > 600 ms.

Figure 9 shows a collection of discharge data that is relevant to SN132800. The HEF interval is marked by a blue vertical bar. As seen in panel (c), the HEF interval is devoid of low frequency n = 1 tearing or kink-type activity and TAE activity is minimal. In panel (b), no apparent impact of the HEF appears on the CAE/GAE modes. Panel (e) shows robust 'Type 1' ELM activity during the HEF. Also, there appears to be a modest but distinct increase in the total neutron yield and stored energy during the HEF. However, as will be shown later in Sec. 5.0 these increases are not caused by the HEF itself. Figure 10 shows the MPTS and CHERS data with the HEF interval again marked by a blue vertical bar. Of note is onset of a strong increase in T_e commencing with onset of the HEF.

3.3 'Tandem' High-Energy Feature: SN128895

A 'tandem' HEF is characterized by two or more events occurring sequentially in time during the same discharge. A representative case in shown in the upper plot of Fig. 11 where a relatively weak initial HEF in the interval t ~ 300 – 500 ms turns off and is then

followed by a more robust HEF in the interval t = 620 – 920 ms identified by the blue circle in on the NPA 3D energetic ion spectrum. The lower plot shows spectra line-outs at t = 600, 700, and 850 ms. As before, it is evident that the HEF occurs at the NB full injection energy, E_b = 90 keV, and not at the NB fractional energies, $E_b/2$ = 45 keV and $E_b/3$ = 30 keV. However, this is a notably rare discharge where a slowing-down distribution does evolve from the HEF energy, albeit over a period of more than 300 ms which is ~ 10x longer than the usual NB slowing-down time. As before, the spectrum was obtained for a NPA tangency radius of R_{tan} = 70 cm that localizes the measurement to the intersection with the NB footprint at a major radius of R_{int} ~ 85 cm. Here attention will be focused on the second HEF evident in the black NPA = 90 keV curve in panel (c) of Fig. 12 marked in time by the vertical blue bar. As seen in panel (b), the second HEF period is devoid of both the f < 10 kHz n = 1 kink-type MHD and the TAE activity. Also, it can be argued that the first HEF period was weaker because of some residual n = 1 activity. Again, panel (a) indicates that robust CAE/GAE activity is unaffected by the HEF. Finally, reappearance of n = 1 modes along with bursting MHD terminates the second HEF at t > 920 ms.

Figure 13 shows a collection of discharge data that is relevant to SN128895. The second HEF interval is marked by the blue vertical bar. As seen in panel (c), the HEF interval is devoid of both low frequency n = 1 kink-type and TAE modes. Panel (b) indicates no impact of the HEF on CAE/GAE modes. Panel (e) shows hashy ELM activity during the HEF as well as a modest but distinct increase in the total neutron yield and stored energy during the HEF as before. Figure 14 shows the MPTS and CHERS data with the HEF interval of interest marked by a blue vertical bar. A significant increase in T_e (as well as n_e) appears to commence with onset of the second HEF.

3.4 'Persistent' High-Energy Feature: SN132928

A 'persistent' HEF is characterized by the absence of a turn-on event and appears to evolve smoothly in time at the NB full energy following the initial NB injection phase. A classic case in shown in the upper plot of Fig. 15 identified by the blue circle in on the NPA 3D energetic ion spectrum. The lower plot shows spectra line-outs at t = 200, 300, 400 and 500 ms. Whereas the spectra show typical depletion down to $E_b/2$ = 45 keV, the HEF at

the NB full injection energy, E_b = 90 keV, exhibits no attenuation whatsoever. An additional point to be made is that the HEF amplitude can be comparable to (but never exceeds) the NPA flux observed in the early stage of NB injection. As before, the spectrum was obtained for a NPA tangency radius of R_{tan} = 70 cm that localizes the measurement to the intersection with the NB footprint at a major radius of $R_{int} \sim 85$ cm. In Fig. 16, the HEF period on the black NPA = 90 keV curve in panel (c) is marked by the vertical blue bar. As seen in panel (b), the HEF period is devoid of the f < 10 kHz n = 1 kink-type MHD but modest TAE activity exists for a period after the HEF onset and arguably is responsible for some 'weakening' of the HEF amplitude in the associated time interval. Finally, reappearance of n = 1 MHD terminates the HEF at t > 600 ms.

Figure 17 shows a collection of discharge data that is relevant to SN128895 with the HEF interval marked by the blue vertical bar. The HEF interval is devoid of low both frequency n = 1 kink-type modes as seen in panel (c) and CAE/GAE modes as seen in panel (b). Panel (e) shows no ELM activity during the HEF. Evolution of the total neutron yield and stored energy during the HEF are obfuscated by NB turn-on and a locked mode event preceding the HEF. Figure 18 shows the MPTS and CHERS data with the HEF interval of interest marked by a blue vertical bar. A significant increase in T_e appears to commence early in the HEF phase as well as a ramp up in n_e.

3.5 'Dual-energy' High-Energy Feature: SN135174

For a few discharges with NB Sources A, B @ 90 keV and C @ 67 keV, HEFs have been observed at both NB full injection energies. The dual-energy HEFs sometimes over lap in time but most often appear sequentially. A clean sequential case with sharp turn-on and turn-off times is shown in the upper plot of Fig. 19 where the E_b = 90 keV HEF occurs first in the interval t ~ 380 – 670 ms (blue encircle) then turns off and is simultaneously followed by the E_b = 65 keV HEF in the interval t ~ 670 – 1000 ms (black encircle) on the NPA 3D energetic ion spectrum. The lower plot shows spectra line-outs at t = 200, 400, and 800 ms.

In Fig. 20, the E_b = 90 keV HEF is demarked by a blue vertical bar and the E_b = 67 keV HEF by a green vertical bar. As seen in panel (b), the E_b = 90 keV HEF occurs during a

period that is devoid of n = 1 modes and exhibits minimal TAE activity. The transition to the E_b = 67 keV HEF is marked by two strong EPM bursts/avalanches that collapse the E_b = 90 keV HEF (and S_n) while generating large spikes in the E_b = 67 keV HEF. Concurrently there is a massive collapse in toroidal rotation velocity, v_ϕ, that drives the strong transition in the CAE/GAE activity seen in panel (a). Following these events the E_b = 90 keV HEF remains suppressed while the E_b = 67 keV HEF continues from t ~ 670 – 1000 ms. The remarkable point here is that the E_b = 67 keV HEF exists in the presence of strong n = 1,2 activity that always destroys the E_b = 90 keV HEF.

Figure 21 shows a collection of discharge data that is relevant to SN135174 with colored vertical bars demarking the times of interest as in the preceding figure. As seen in panel (c), the E_b = 90 keV HEF interval is devoid of low frequency n = 1 kink-type modes and has only weak TAE activity while the inverse occurs during the E_b = 67 keV HEF. At the transition between E_b = 90 keV and E_b = 67 keV HEFs, panel (b) shows a strong change CAE/GAE activity that coincides with an abrupt collapse in toroidal rotation velocity, v_ϕ, but again the HEFs do not appear to drive any significant fluctuations or modulation of the CAE/GAE activity. Panel (e) shows sporadic ELM activity during both HEFs but possible changes in the total neutron yield and stored energy are obfuscated by preceding events. Figure 22 shows the MPTS and CHERS data with the HEF intervals marked as before. A significant increase in T_e appears to commence around the time of transition between the dual-energy HEFs.

4.0 Summary of Parametric Dependencies of the High-Energy Feature

A summary of the NSTX operational scenarios, plasma discharge parameters and diagnostic characteristics related to observation of the High-Energy Feature is presented below.

- EIIB NPA Observations

The HEFs are observed as a transient increases in the NPA charge exchange flux localized at the NB full energy (never at the NB fractional energies) that exhibit rise-times

of ~ 20 – 80 ms and durations up to 100's of milliseconds. HEFs can turn on and off multiple times during a single discharge.

The NPA detector is a multi-anode microchannel plate array. By adjusting the analyzer E||B fields, the HEF is observed to move to different detector anodes in agreement with the energy calibration which provides definitive confirmation that the HEF is not a NPA instrumental effect.

HEFs have been observed for mid-plane NPA sightlines with: R_{tan} ~ 55 – 90 cm corresponding to $v_{||}/v$ ~ 0.7 – 0.9: i.e. for passing energetic ions but not trapped. No systematic horizontal scans are available. The magnitude of the HEF flux can approach (but not exceed) that of NBI spectrum early in the discharge. Ions are not accelerated above NB injection energy. Evolution of a slowing-down distribution below the HEF is only rarely observed and then the evolution is very slow (100's ms) compared with normal beam slowing down times (10's ms).

• Global Discharge Conditions

The HEF is observed only in H-mode discharges (never L-modes) but not under all H-mode conditions. At a minimum, it is also required that $P_b \geq 4$ MW. Short, shabby H-mode discharges with $P_b << 4$ MW plagued by early locked-mode events have been generated by manipulation of the NB power evolution and other discharge conditions. However, HEFs have never been observed under these conditions.

As can be seen in Table I, HEFs are observed mostly for $B_T = 4.5$ kG (with a few cases for $B_T = 5.0, 5.5$ kG) and $I_p = 0.8 – 1.2$ MA (not with lower I_p, B_T operation). HEF onset most frequently occurs during mid-discharge: e.g. $t > 0.4$ s and $n_e \geq 5x10^{13}$ cm^{-3}. HEFs are observed with and without operation of the NSTX error field correction coils. Core-carbon accumulation appears to grow during the HEF period.

• MHD Behavior

The HEF is not observed in the presence of $f < 10$ kHz tearing or kink-type modes except for the lower energy $E \leq 70$ keV cases. HEF appearance also requires a reduced level of $f < 140$ kHz TAE activity. MHD bursting events (e.g. EPM/TAE as well as IREs

and/or sawteeth) modulate a wide range of energies including the HEF and usually terminate the HEF event. The RMS amplitude of the Mirnov signal in the CAE/GAE frequency range 400 – 1500 kHz does not show any signatures correlating with the HEF.

• ELM Effects

HEFs can occur with (e.g. SN132800) or without (e.g. SN132928) ELM activity. When present, ELMs can modulate the HEF amplitude by up to ~ 30%: e.g. SN132800 with ~ 200 Hz ELMs. The increase in HEF flux lags the ELM by ~ 3-5 ms. This suggests that the ELMs release neutrals from the wall which then propagate into the plasma periphery causing increased charge exchange flux. This also suggests that the HEF orbits transit in both the plasma core and peripheral regions.

• Lithium Deposition Effects

No HEFs are observed when Lithium deposition using the Lithium Evaporator (LiTER) exceeds ~ 150 mg/shot or levels typically sufficient to suppress ELM activity [35, 36]. The HEFs progressively disappeared as Lithium deposition is increased to the noted level and can reappear as Lithium effects wear off. The same behavior is observed when Lithium is applied using the 'dropper' technique. Why Lithium deposition affects the HEF behavior is not understood.

5.0 TRANSP Code Analysis

The TRANSP code [37] is capable of simulating the NPA neutral flux measurements including horizontal and vertical scanning. In the following analysis, the TRANSP option to follow the fast ion gyro-orbit is used (as opposed to the guiding center).

As shown in the upper plot of Fig. 23, the High-Energy Feature (HEF) does not appear on the TRANSP-simulated NPA spectrum. This is consistent with the conjecture that the HEF is a wave-particle interaction phenomenon since TRANSP knows nothing about MHD activity. The lower plot shows that TRANSP closely reproduces in time evolution and magnitude the excursions in S_n and W_T observed in measurements. It will be

demonstrated momentarily that the changes in S_n and W_T are driven by increases in the core T_e, n_e, T_i and n_D (all of which are measured inputs except n_D) that are reflected by increases in the calculated core total energy density and beam-target neutron yield. The ion power balance is 'normal' with the most significant change being a decrease in +QIE during the HEF time-of-interest.

Figure 24 serves to demonstrate that the above behavior of S_n and W_T is not related to the HEF phenomenon. SN132181 is a HEF-free discharge with a strong increase in measured and calculated S_n and W_T as seen in panel (e) that occur in the interval marked by the vertical gray bar. Panel (c) shows that this interval is devoid of n = 1 kink-type MHD and the TAE activity is minimal as occurs in discharges with HEF events. The NPA energetic ion contour plot in panel (d) does not exhibit enhanced flux at the NB injection energy: i.e. the discharge is HEF-free. A strong increase in electron temperature concurrent with the increases in S_n and W_T is evidenced in panel (b). Though not shown, concurrent significant increases also occur in the measured core n_e, T_i and v_ϕ. This leads to the conclusion that the S_n and W_T excursions are driven by plasma profile changes rather than the HEF. The tentative interpretation is that reduced low-f MHD activity results in improved confinement that, in turn, is the driver for plasma profile changes producing the excursions in the measured and calculated S_n and W_T parameters.

6.0 Discussion

The HEF has not been clearly observed on NSTX energetic ion diagnostics other than the E||B NPA, such as the Fast-ion D-alpha (FIDA) [38], scintillator Fast-Loss Ion Probe, (sFLIP) [27] and the solid state Neutral Particle Analyzer (ssNPA) [39].

The FIDA diagnostic array has sightlines with semi-vertical views through the NB footprint that constrain the measurements to the pitch range $v_{||}/v \sim 0.1 - 0.7$: i.e. to predominantly trapped energetic ions. Recall that the E||B NPA has observed HEFs for mid-plane NPA sightlines in the pitch range $v_{||}/v \sim 0.7 - 0.9$: i.e. only for passing particles.

If one assumes that the HEF phenomenon is constrained to passing energetic ions, then it is understandable that this feature is not observed by the FIDA diagnostic.

The sFLIP diagnostic views energetic ion loss orbits that intersect the NSTX outboard wall. However, the neutron diagnostics never show any 'dip' indicative of particle loss attending the HEF period. Thus one can conclude that the HEF is not an ion loss phenomenon and hence the absence of sFLIP signals is understandable.

The ssNPA diagnostic is a mid-plane 4-chord array with fixed tangency radii of R_{tan} = 60, 90, 100 and 120 cm. Except for the 120 cm chord, the sightlines intersect the NB footprint which constrains the measurements spatially as well as in pitch range to $v_{||}/v \sim 0.4 - 0.8$. Each chord views an energy range of $E \sim 30 - 100$ keV that is divided into seven energy windows of width $\Delta E \sim 10$ keV. While the ssNPA chord at R_{tan} = 90 cm occasionally shows some indication of HEF phenomenon, the relatively large energy window leads to a smoothing of the signal that obscures the distinct turn-on and turn off characteristics seen on the EIIB NPA. Within these limitations, it can be said that the ssNPA diagnostic supports the EIIB observations but lack temporal detail.

It was pointed out earlier that (in addition to certain MHD behavior) the occurrence of HEFs required existence of a H-mode discharge *and* injected beam power $P_b \geq 4$ MW. However, it should be noted that these are not independent conditions. At $P_b \geq 4$ MW, NSTX discharges routinely undergo an early L-H transition unless special steps are taken to suppress the transition.

A phenomenon bearing similarities to the HEF observed on NSTX has been reported for NPA energetic ion spectra measured on START [19] in discharges heated using 30 keV hydrogen NBI. Termed a 'bump-on-tail', the START spectra exhibit a variation with energy that is significantly more gradual compared with the spike-on-tail' characteristic of the HEF in NSTX. Although energetic particle-driven instabilities are invoked as a contributing mechanism on START, a significant role is also attributed to orbit excursions well beyond the separatrix combined with the high atomic and molecular density enveloping the plasma that can result in a depletion of the energetic ion population during the slowing down process leaving the noted 'bump-on-tail' in the full energy region of the spectrum. Such orbit excursion effects do not play a significant role in NSTX

because of the short distance between the separatrix and the vacuum vessel internal structures.

Though a definitive mechanism has yet to be developed for NSTX, the HEF appears to be caused by a form of TAE/CAE wave-particle interaction that distorts the NB fast ion distribution in phase space. As a starting point, TRANSP is used to examine the $f_i(E,v_{||}/v)$ distribution localized along the NPA line-of-sight to a volume defined by its intersection with the NB footprint. Unfortunately, TRANSP has no first-principle model for wave-particle driven effects on energetic ions nor any other mechanism like large-angle Coulomb scattering that could increase both the energy diffusion and pitch-angle scattering, so the TRANSP $f_i(E,v_{||}/v)$ distribution only provides a baseline for additional analysis. The next step is to import the TRANSP $f_i(E,v_{||}/v)$ along with a model for the CAE/GAE eigenmodes from say NOVA into a new code called SPIDLE that has been developed by G. Kramer at PPPL. SPIDLE evolves the $f_i(E,v_{||}/v)$ distribution in the presence of background plasma profiles under the drive from wave-particle interactions such as CAE/GAE eigenmodes. However, extensive application of the SPIDLE code to the HEF topic cannot occur until later this year so this work will be presented in a future document.

References

[1] M. Ono, *et al.,* "Overview of the Initial NSTX Experimental Results," Nucl. Fusion **41**, (2001) 1435

[2] Y.-K. M. Peng and D. J. Strickler, Nucl. Fusion **26**, (1986) 769

[3] J. E. Menard, *et al.,* "β-Limiting MHD Instabilties in Improved-performance NSTX Spherical Torus Plasmas," Nucl. Fusion **43**, (2003) 330

[4] J. E. Menard, *et al.,* "Overview of Recent Physics Results from the National Spherical Torus Experiment (NSTX)," Nucl. Fusion **47**, (2007) S645

[5] D. A. Gates, *et al.,* "Overview of Results from the National Spherical Torus Experiment (NSTX)," Nucl. Fusion **49**, (2009) 104016

[6] S. M. Kaye, *et al.,* "Progress Towards High Performance Plasmas in the National Spherical Torus Experiment (NSTX)." Nucl. Fusion **45**, (2005) S168 – S180

[7] C. Z. Cheng and M. S. Chance, Phys. Fluids **29**, (1986) 2471

[8] E. D. Fredrickson, N. N. Gorelenkov, D. Darrow, *et al.*, "Wave Driven Fast Ion Loss in the National Spherical Torus Experiment," Phys. of Plasmas **10**, (2003) 2852

[9] H. L. Berk, B. N. Breizman, J. Candy, *et al.*, "Spontaneous Hole-clump Pair Creation," Phys. Plasmas **6**, (1996) 3102

[10] E. D. Fredrickson, *et al.*, "Scaling of Kinetic Instability Induced Fast Ion Losses in NSTX," 20th IAEA Fusion Energy Conference, Vilamoura, Portugal, 1-6 November 2004 (IAEA, Vienna) CD-ROM EX/5-3. Also Princeton Plasma Physics Laboratory Report, PPPL-4084 (2005).

[11] S. S. Medley*, et al.*, "MHD-Induced Energetic Ion Loss during H-mode Discharge in the National Spherical Torus Experiment," Nucl. Fusion **44**, (2004) 1158

[12] J. E. Menard, *et al.*, "Observation of Instability-Induced Current Redistribution in a Spherical Torus Plasma," Phys. Rev. Lett. **97**, (2006) 095022

[13] M. Garcia-Munoz, *et al.*, "NTM induced Fast-ion Losses in ASDEX Upgrade," Nucl. Fusion **47**, (2007) L10

[14] M. Garcia-Munoz, *et al.*, "MHD induced Fast-ion Losses on ASDEX Upgrade," Nucl. Fusion **49**, (2009) 085014

[15] W. W. Heidbrink, N. N. Gorelenkkov, M. Murakami, “Beam-Driven Energetic Particle Modes in Advanced Tokamak Plasmas,” Nucl. Fusion **42**, (2002) 972

[16] K. L. Wong, *et al.*, “Internal Transport Barrier Driven by Redistribution of Energetic Ions,” Nucl. Fusion **45**, (2005) 30

[17] S. S. Medley, D. S. Darrow, D. Liu and A. L. Roquemore, “Prompt Loss of Energetic Ion during Early Neutral Beam Injection in the National Spherical Torus Experiment,” Princeton Plasma Physics Laboratory Report, PPPL-4060 (2005)

[18] D. S. Darrow, *et al.*, “Fast Ion Loss Diagnostic Plans for the National Spherical Torus Experiment,” Rev. Sci. Instrum. **72**, (2001) 784

[19] K. G. McClements, *et al.,* “Physics of Energetic Particle-Driven Instabilities in the START Spherical Tokamak,” Plasma Phys. Control. Fusion **41**, (1999) 661

[20] E. D. Fredrickson, L. Chen and R. B. White, “Bounce Precession Fishbones in the National Spherical Torus Experiment,” Nucl. Fusion **43**, (2003) 1258

[21] N. N. Gorelenkov, *et al.,* “Beam Ion Driven Instabilities in the National Spherical Torus Experiment,” Phys. Plasmas **11**, (2004) 2586

[22] E. D. Fredrickson, *et al.*, “Fast Ion Loss in a ‘Sea-of-TAE’,), Nucl. Fusion **47**, (2006) S926 – S93

[23] E. D. Fredrickson, *et al.*, “Modeling Fast-ion Transport during Toroidal Alfven Eigenmode Avalanches in National Spherical Torus Experiment,” Phys. Plasmas **16**, (2009) 122505

[24] R. J. Akers, *et al.,* “Neutral Beam Heating in the START Spherical Tokamak,” Nucl. Fusion **42**, (2002) 122

[25] R. J. Akers, *et al.,* “Transport and Confinement in the Mega Ampere Spherical Tokamak (MAST) Plasma,” Plasma Phys. Control. Fusion **45**, (2003) A175

[26] M. R. Tournianski, *et al.,* “Anisotropic Fast Neutral Spectra in the MAST Spherical Tokamak,” Plasma Phys. Control. Fusion **47**, (2005) 671

[27] D. S. Darrow, “Scintillator Based Energetic Ion Loss Diagnostic for the National Spherical Torus Experiment,” Rev. Sci. Instrum. **79**, (2008) 023502

[28] W. W. Heidbrink, *et al.*, “The Confinement of Dilute Populations of Beam Ions in the National Spherical Torus Experiment,” Nucl. Fusion **43**, (2003) 883

[29] J. E. Menard, *et al.*, "Internal Kink Mode Dynamics in High-β NSTX Plasmas," Nucl. Fusion **45**, (2005) 539

[30] S. S. Medley, *et al.*, "Status of Recent Experimental and Analytical Investigation of MHD-induced Energetic Ion Redistribution or Loss in the National Spherical Torus Experiment," Princeton Plasma Physics Laboratory Report, PPPL-4235 (2007)

[31] S. S. Medley, *et al.*, "Neutral Particle Analyzer Vertically Scanning Measurements of MHD-induced Energetic Ion Redistribution or Loss in the National Spherical Torus Experiment," Princeton Plasma Physics Laboratory Report, PPPL-4270 (2007)

[32] S. S. Medley, *et al.*, "Invited Review Article: Contemporary Instrumentation and Application of Charge Exchange Neutral Particle Diagnostics in Magnetic Fusion Energy Experiments," Rev. Sci. Instrum. **79**, (2008) 011101

[33] S. S. Medley and A. L. Roquemore, "Neutral Particle Analyzer Diagnostic on in the National Spherical Torus Experiment," Rev. Sci. Instrum. **75**, (2004) 3625

[34] S. S. Medley and A. L. Roquemore, "Construction and Operation of Parallel Electric and Magnetic Field Spectrometers for Mass/Energy Resolved Multi-Ion Charge Exchange Diagnostics on the Tokamak Fusion Test Reactor," Rev. Sci. Instrum. **69**, (1998) 2651

[35] H. W. Kugel, *et al.*, "The Effect of Lithium Surface Coatings on Plasma Performance in the National Spherical Torus Experiment," Phys. Plasmas **15**, (2008) 056118

[36] M. G. Bell, *et al.*, "Plasma Response to Lithium-coated Plasma-facing Components in the National Spherical Torus Experiment," Plasma Phys. Control. Fusion **51**, (2009) 124054

[37] J. Onega, M. Evrard, D. McCune, "Numerical Transport Codes," Transactions of Fusion Technology **33**, (1998) 181

[38] M. Podestà, *et al.*, "Experimental Studies on Fast-ion Transport by Alfvén Wave Avalanches on the National Spherical Torus Experiment," Phys. Plasmas **16**, (2009) 056104

[39] D. Liu, *et al.*, "Profiles of Fast Ions that are accelerated by High Harmonic Fast Waves in the National Spherical Torus Experiment," Plasma Phys. Control. Fusion **52**, (2010) 025006

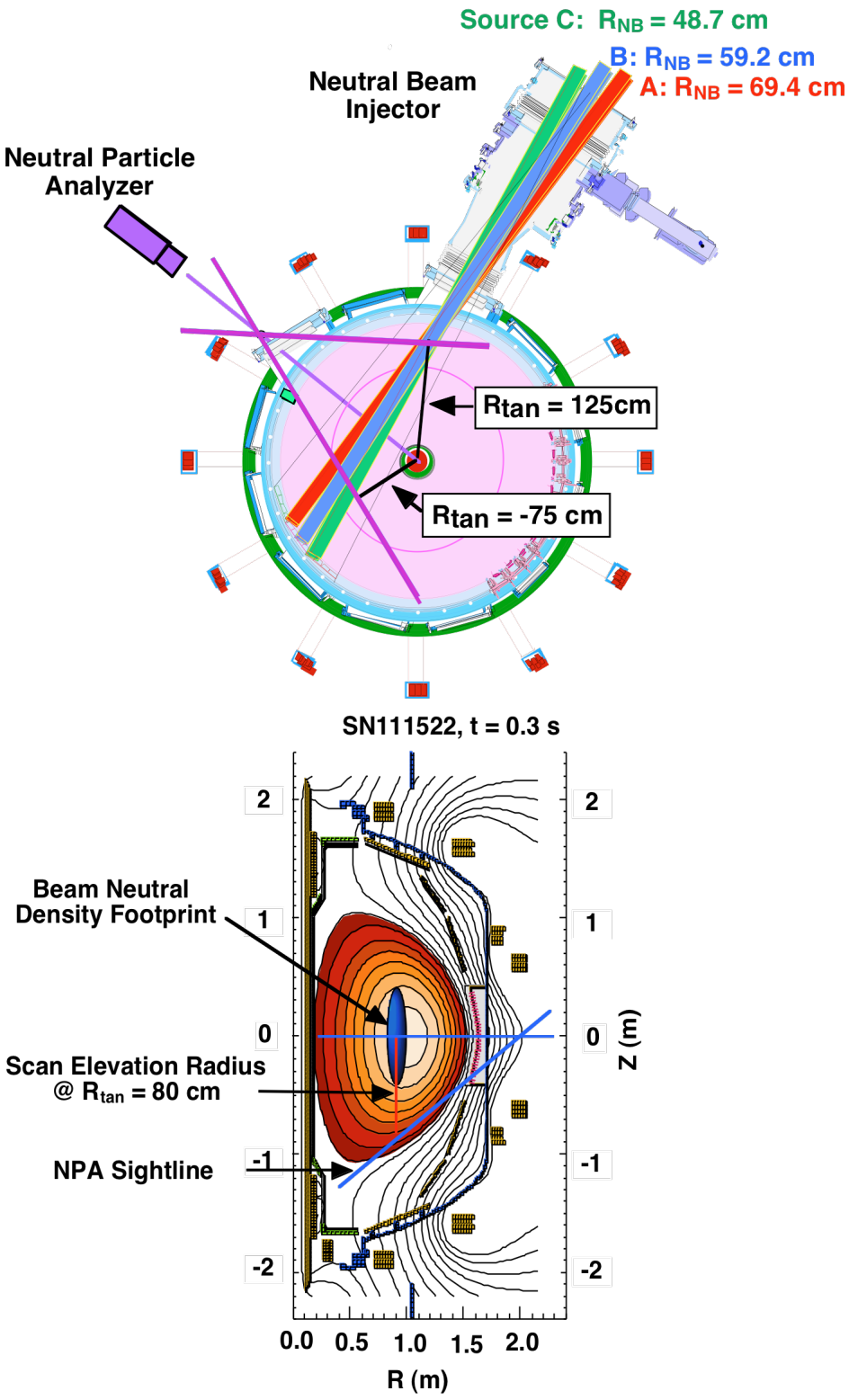

Fig. 1. The Neutral Particle Analyzer (NPA) on NSTX views across the three neutral beam injection sources and can be scanned horizontally (top) over a wide range of sightline tangency radii, R_{tan}, as well as vertically (bottom) on a shot-to-shot basis. R_{tan}, is the perpendicular distance between the machine center and the NPA sightline.

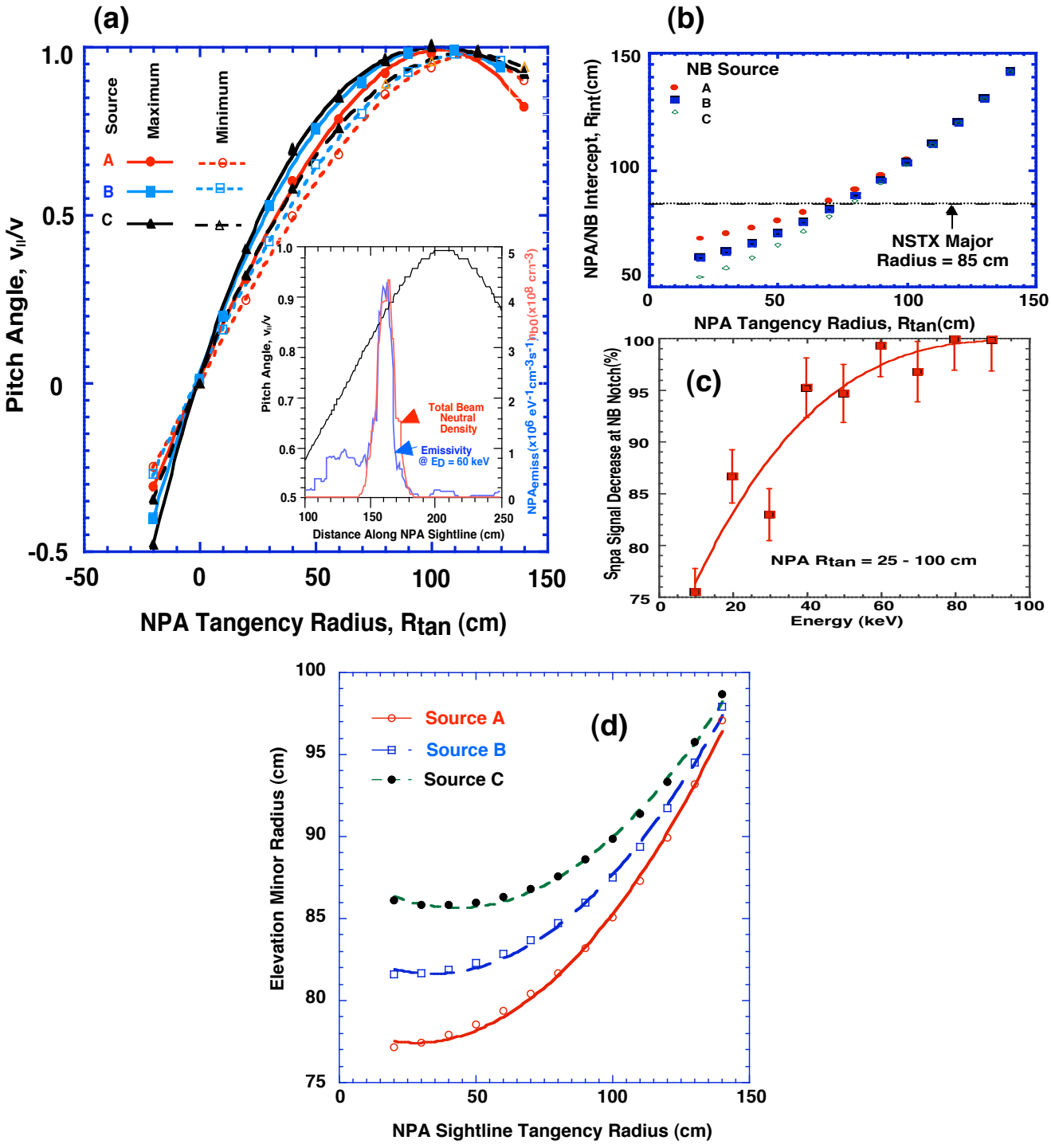

Fig. 2. Pitch angle (left panel) and spatial (upper right panel) localization of the NPA flux arises from the intersection of the diagnostic sightline with the NB sources. Localization is strongest near the NB full energy, but remains substantial over the entire slowing down distribution. The maximum elevation minor radius accessible for vertical scanning depends on the choice of horizontal tangency radius (bottom panel).

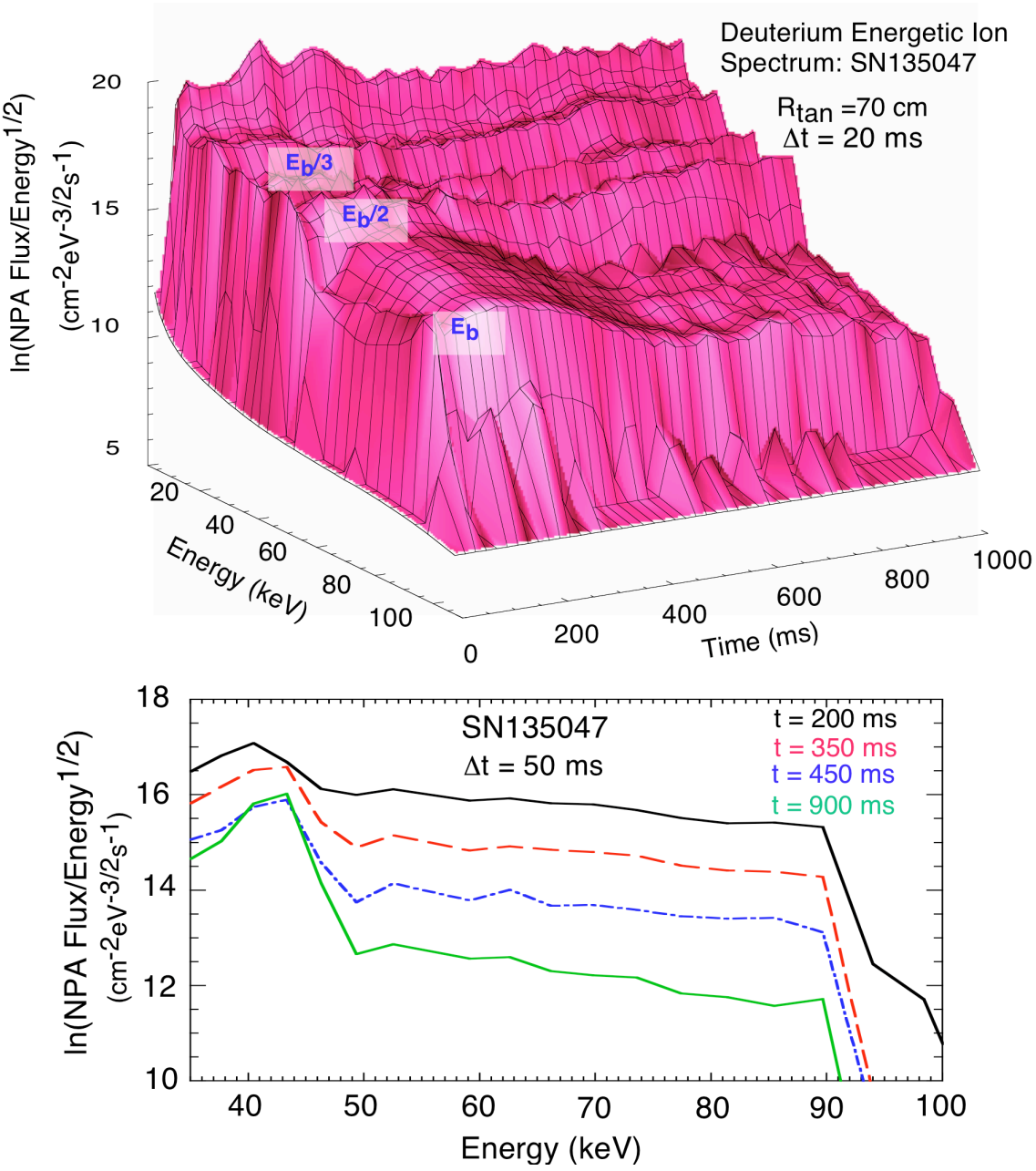

Fig. 3. NPA energetic ion measurements for SN135047 with the NB full, half and third injection energies indicated on the 3D distribution (top) and 2D energy spectrum lineouts at selected times during the discharge (bottom).

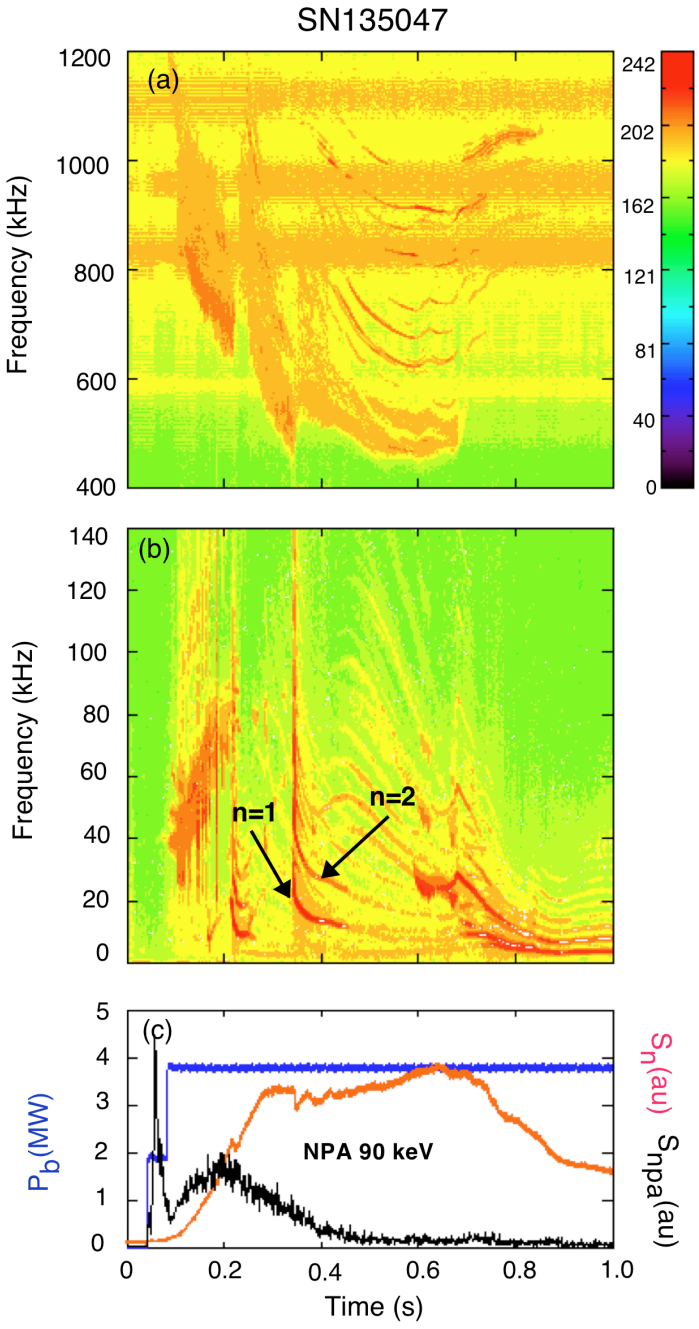

Fig. 4. Mirnov spectrograms for SN135047 in the CAE/GAE (a) and the NTM/TAE (b) regimes plus waveforms showing the injected NB power, NPA signal at E = 90 keV and the volume neutron yield (c).

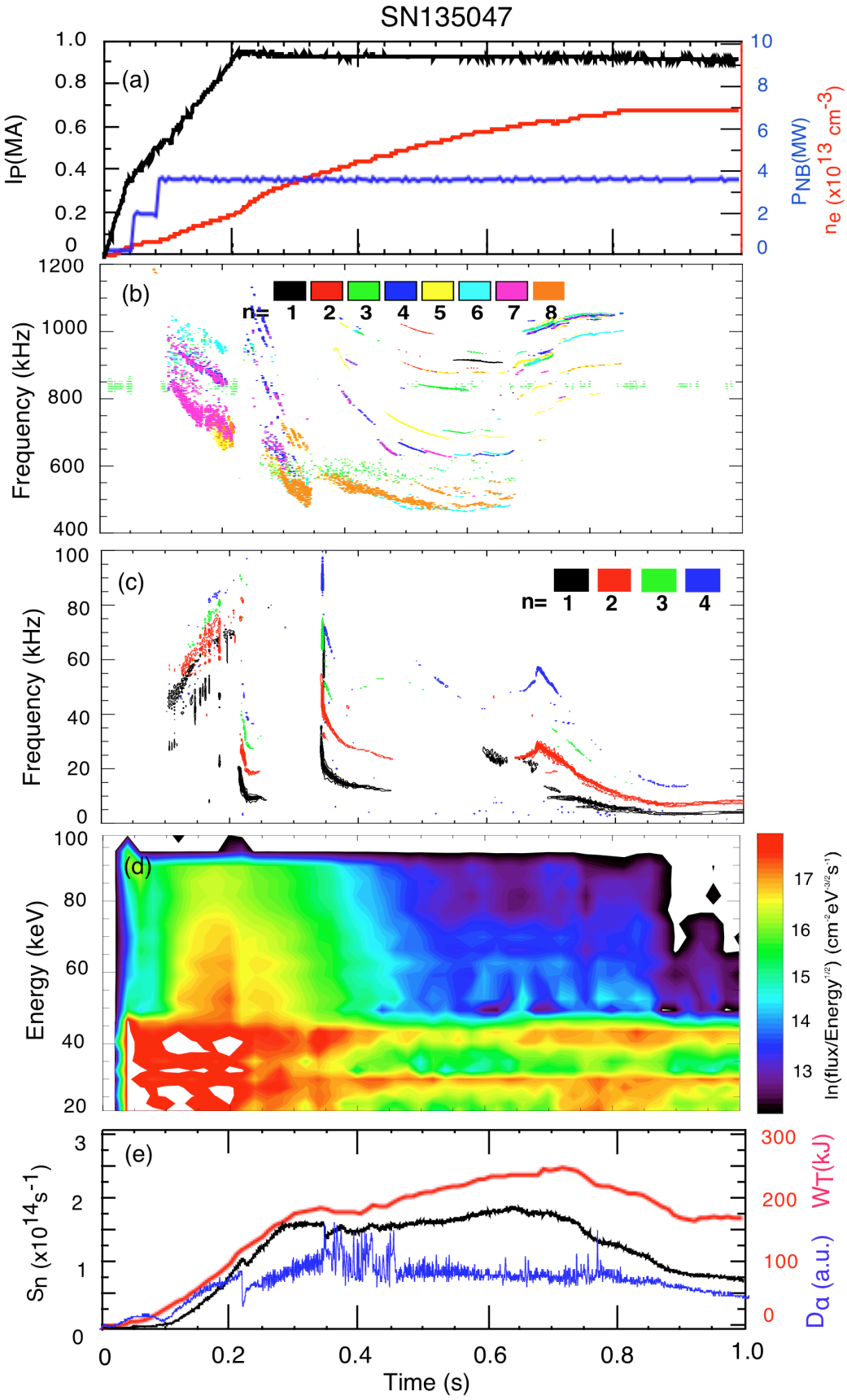

Fig. 5. Selected plasma discharge data for SN135047: (a) plasma current, injected NB power and MPTS line-average electron density, (b) MHD mode analysis for the CAE/GAE regime, (c) MHD mode analysis for the NTM/TAE regime, (d) contour plot of the NPA energetic ion spectrum and (e) volume neutron yield, total stored energy and D_α emission.

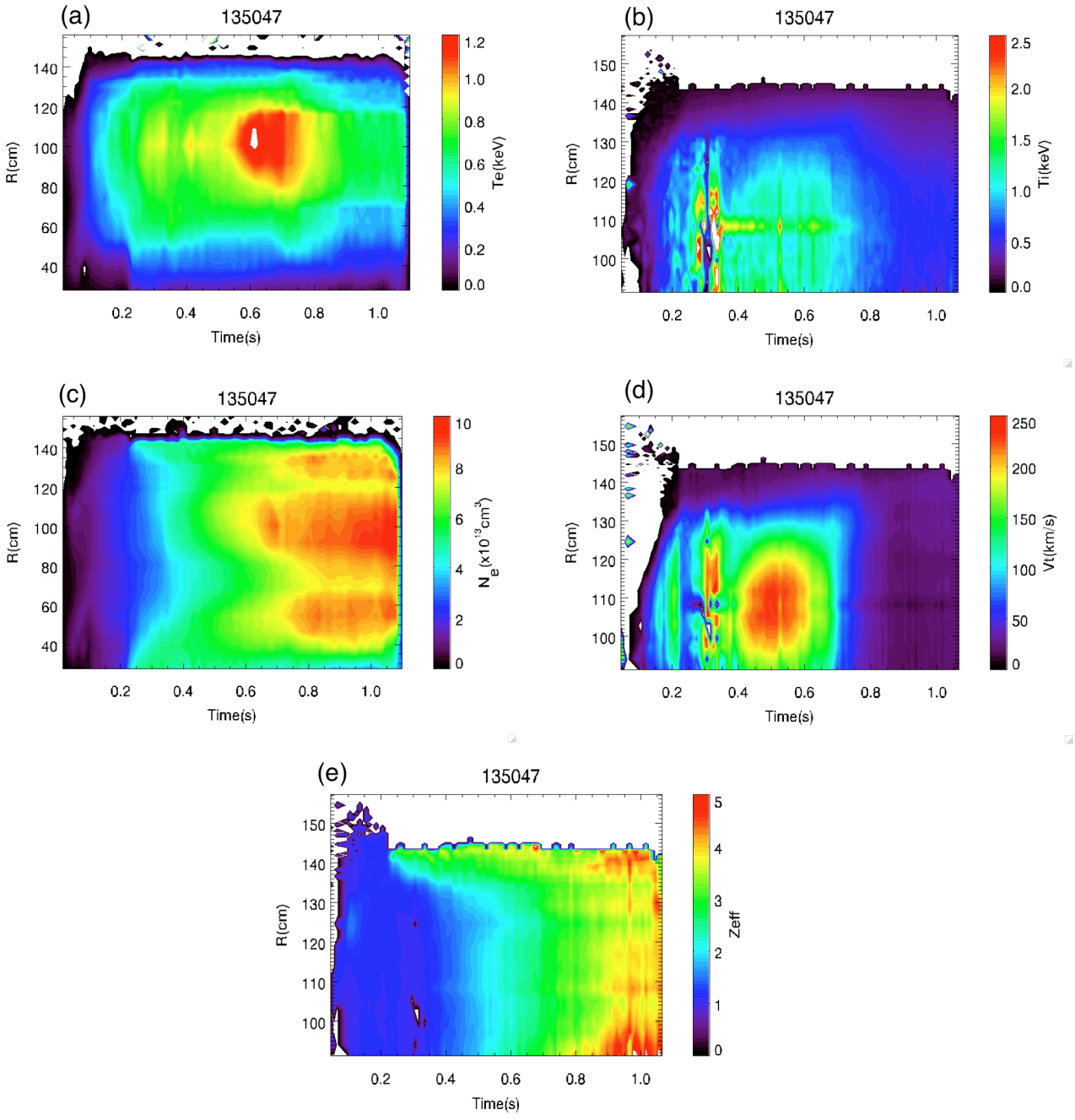

Fig. 6. MPTS and CHERS contour plots for SN135047: (a) electron temperature, (b) deuterium ion temperature, (c) electron density, (d) toroidal rotation velocity and (e) carbon Z_{eff}.

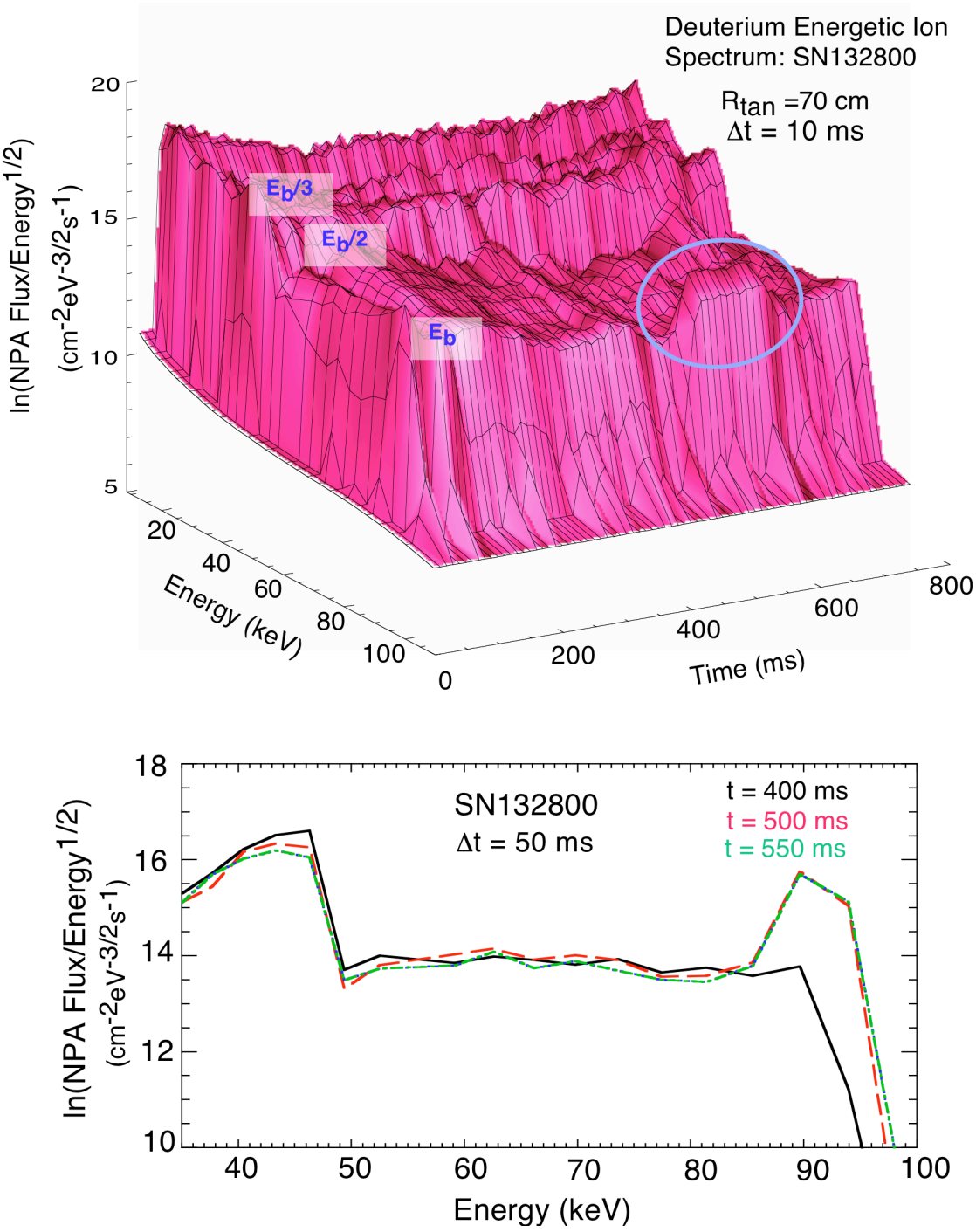

Fig. 7. NPA energetic ion measurements for SN132800 with the NB full, half and third injection energies indicated on the 3D distribution (top) and 2D energy spectrum lineouts at selected times during the discharge (bottom).

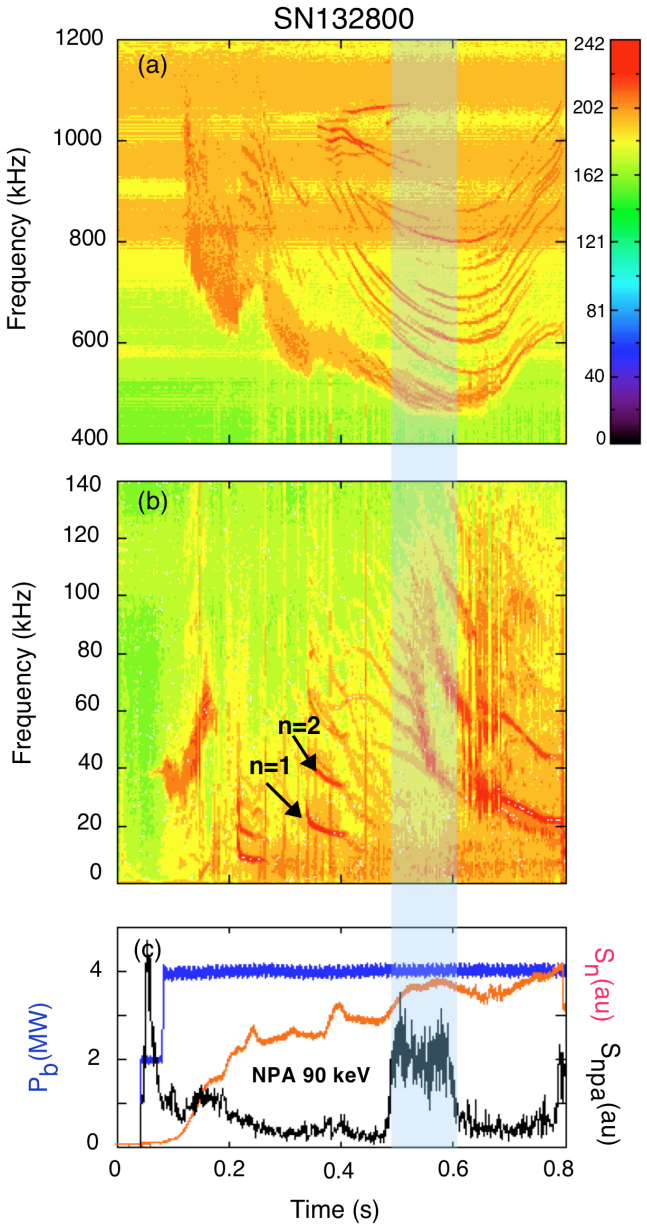

Fig. 8. Mirnov spectrograms for SN132800 in the CAE/GAE (a) and the NTM/TAE (b) regimes plus waveforms showing the injected NB power, NPA signal at E = 90 keV and the volume neutron yield (c).

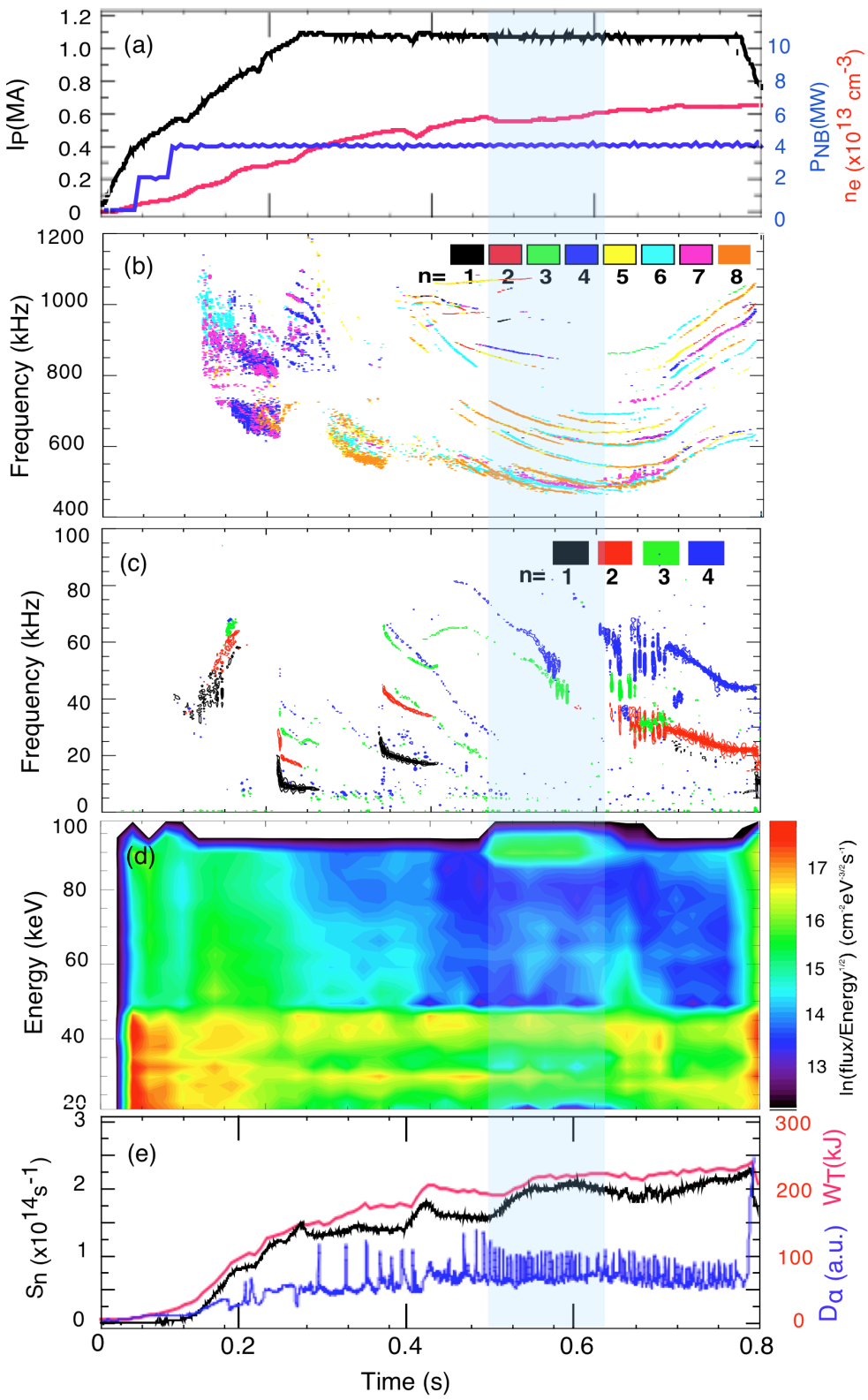

Fig. 9. Selected plasma discharge data for SN132800: (a) plasma current, injected NB power and MPTS line-average electron density, (b) MHD mode analysis for the CAE/GAE regime, (c) MHD mode analysis for the NTM/TAE regime, (d) contour plot of the NPA energetic ion spectrum and (e) volume neutron yield, total stored energy and D_α emission.

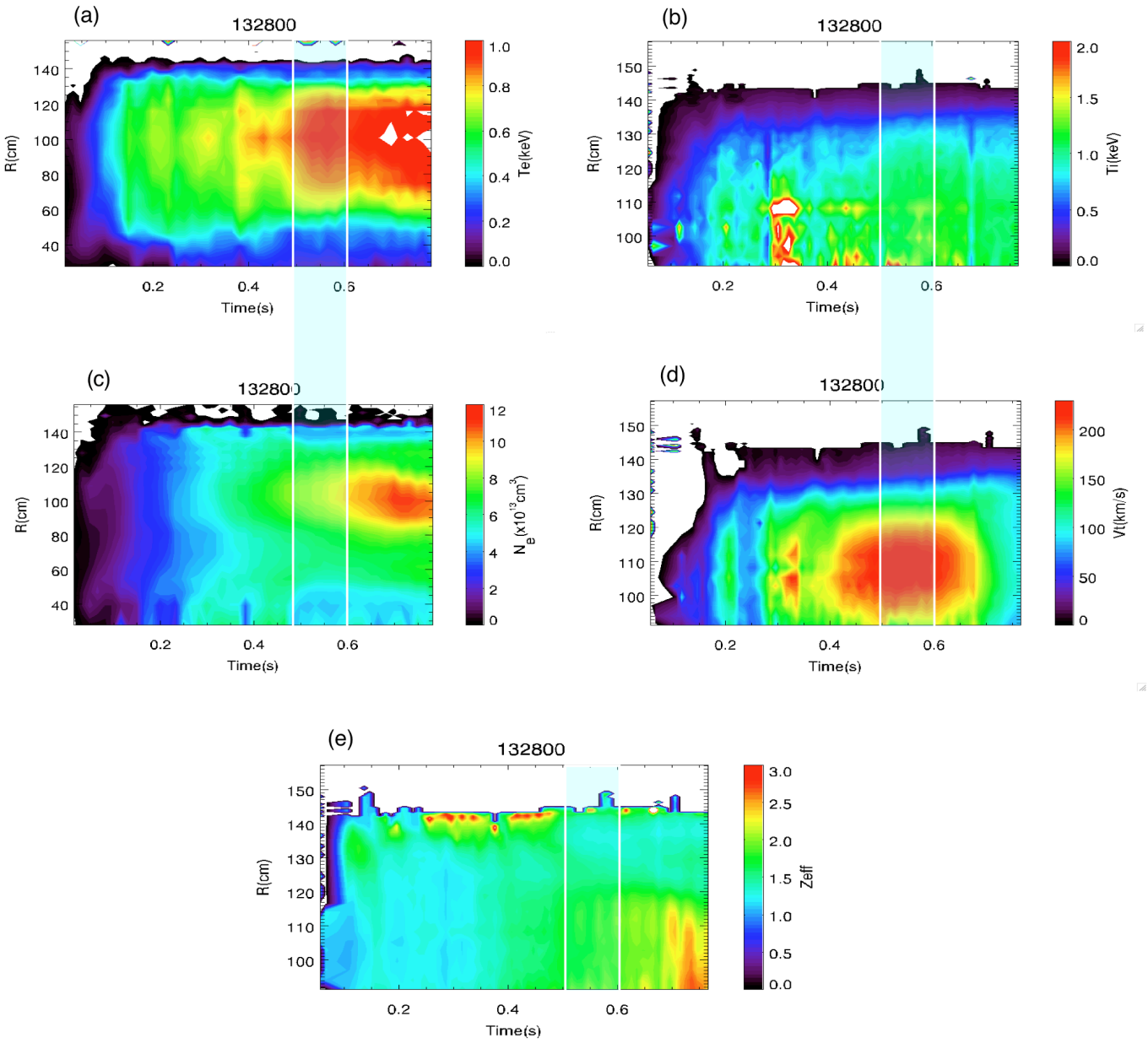

Fig. 10. MPTS and CHERS contour plots for SN132800: (a) electron temperature, (b) deuterium ion temperature, (c) electron density, (d) toroidal rotation velocity and (e) carbon Z_{eff}.

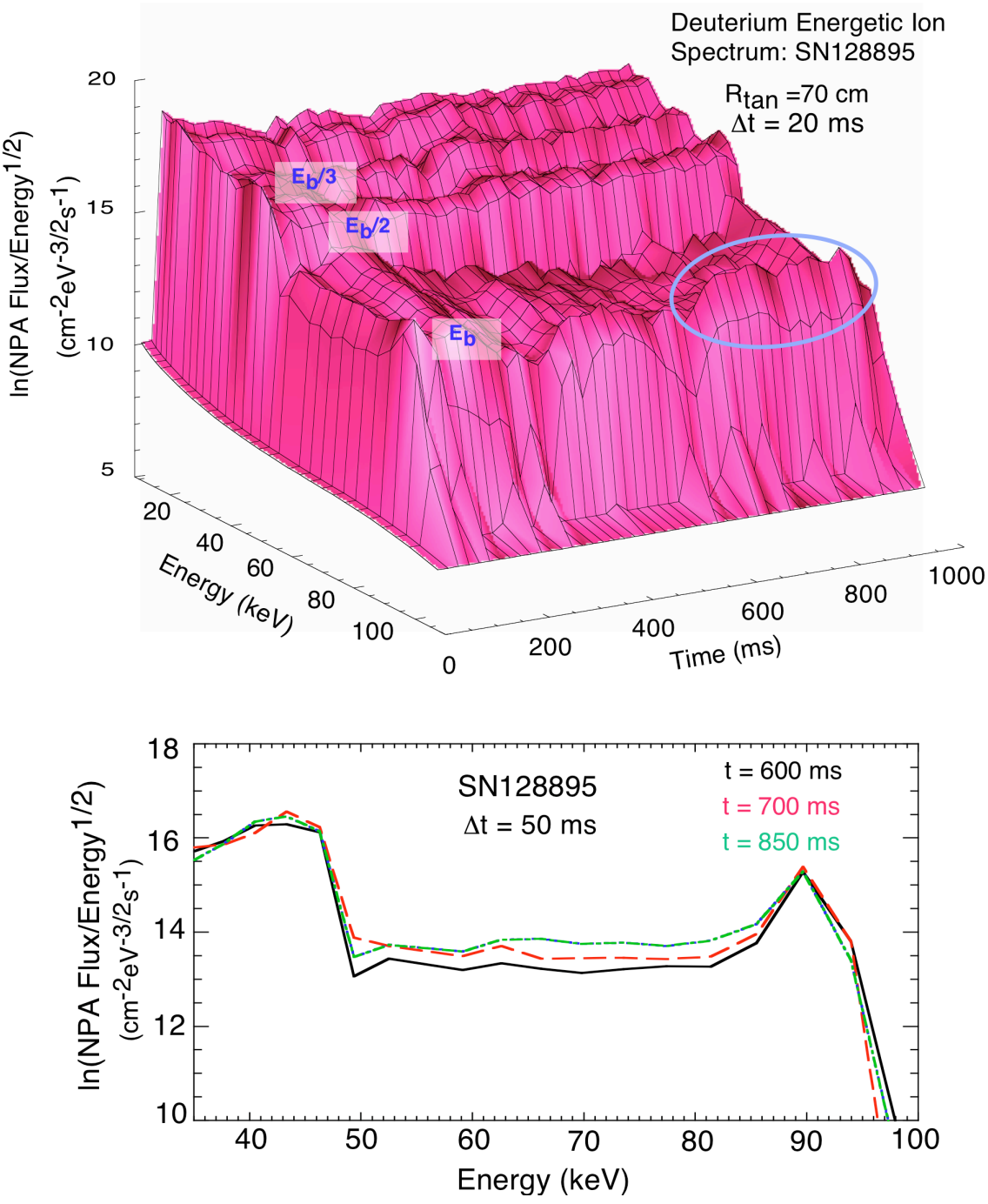

Fig. 11. NPA energetic ion measurements for SN128895 with the NB full, half and third injection energies indicated on the 3D distribution (top) and 2D energy spectrum lineouts at selected times during the discharge (bottom).

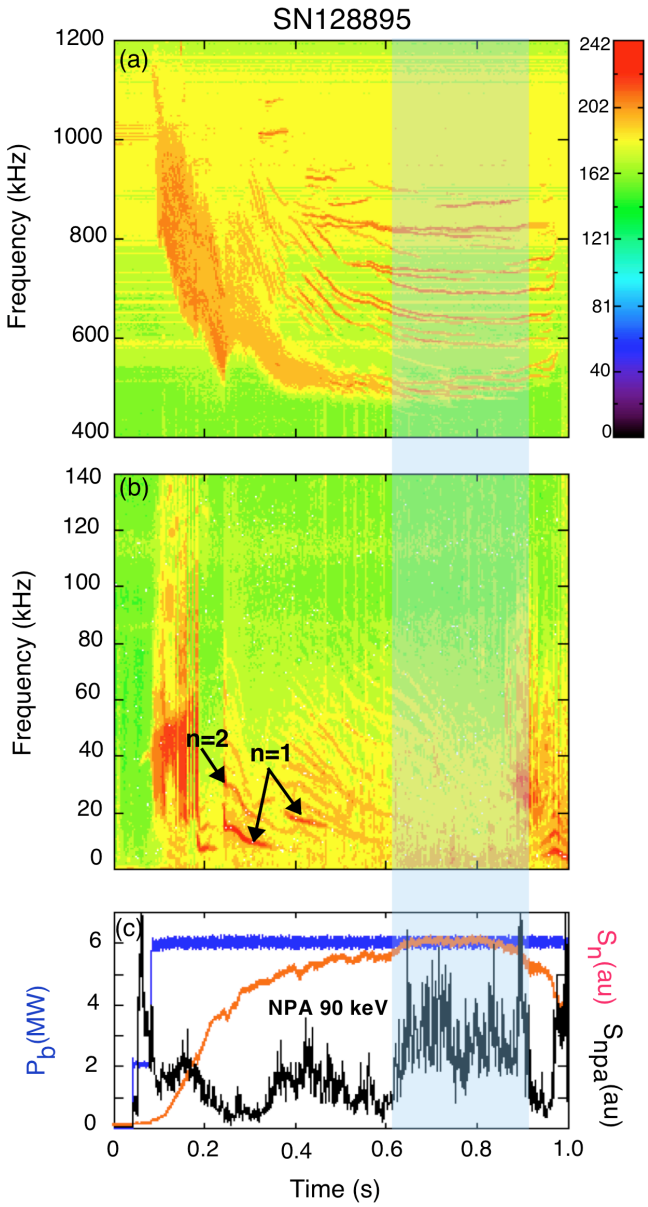

Fig. 12. Mirnov spectrograms for SN128895 in the CAE/GAE (a) and the NTM/TAE (b) regimes plus waveforms showing the injected NB power, NPA signal at E = 90 keV and the volume neutron yield (c).

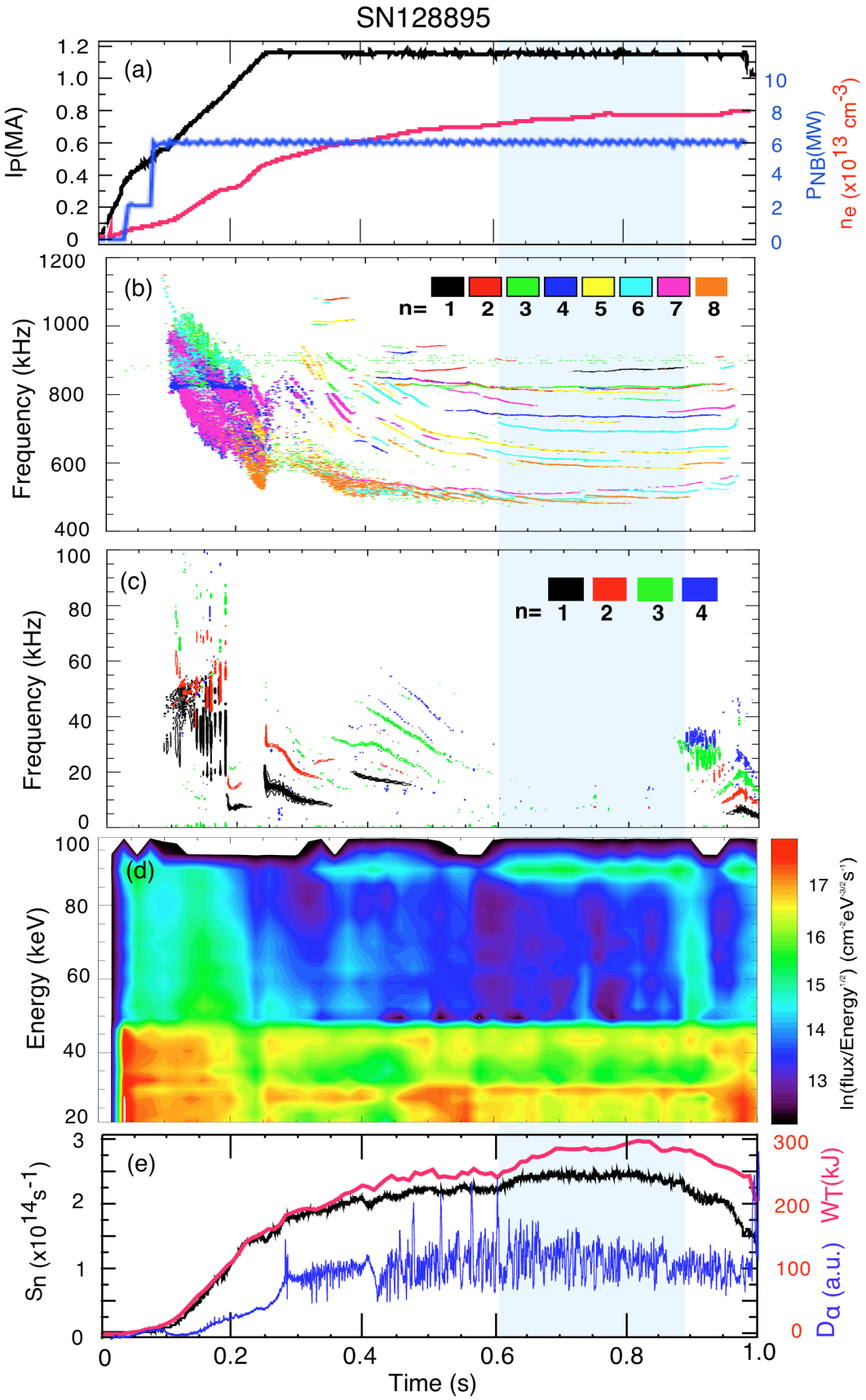

Fig. 13. Selected plasma discharge data for SN128895: (a) plasma current, injected NB power and MPTS line-average electron density, (b) MHD mode analysis for the CAE/GAE regime, (c) MHD mode analysis for the NTM/TAE regime, (d) contour plot of the NPA energetic ion spectrum and (e) volume neutron yield, total stored energy and D_α emission.

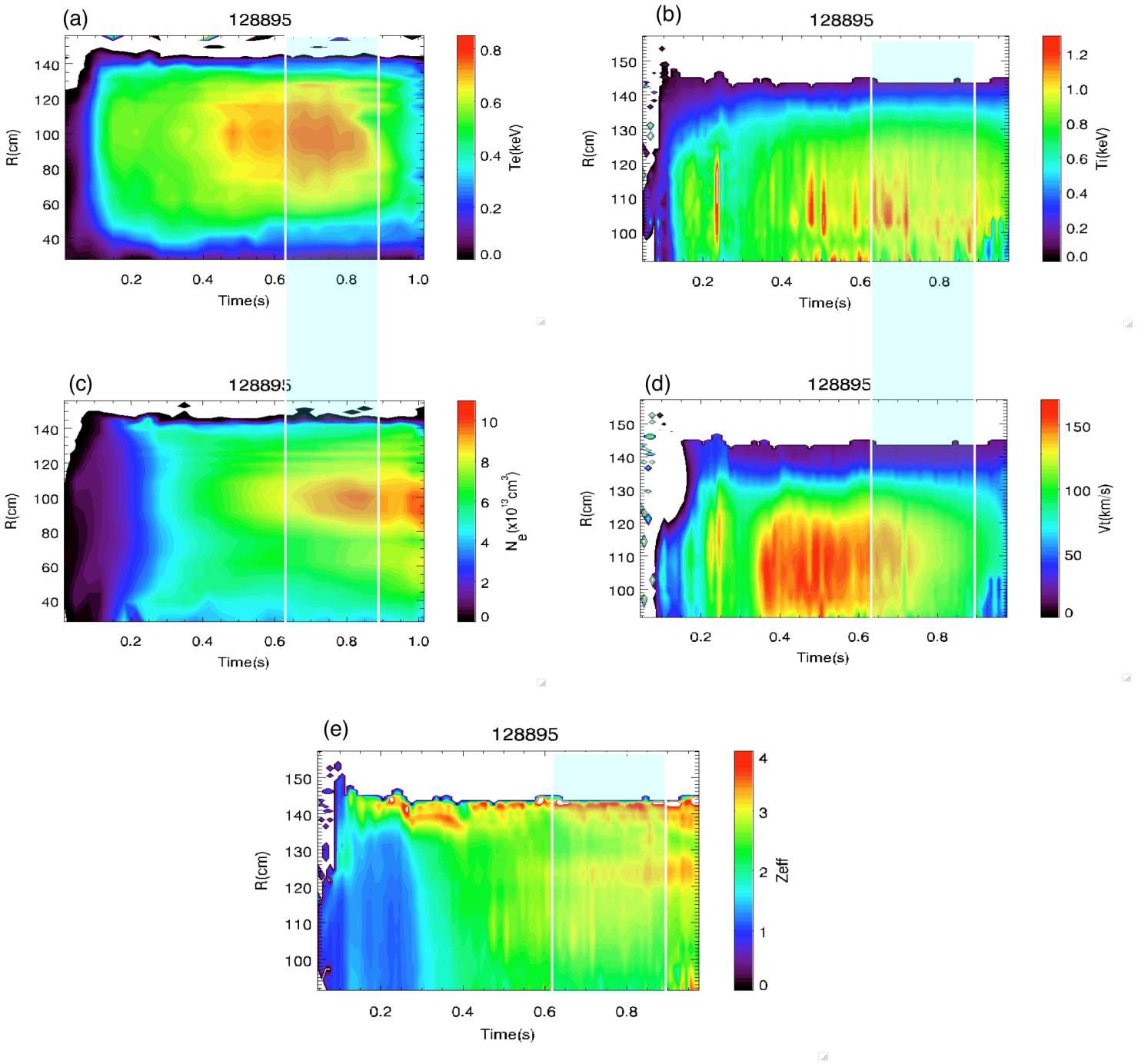

Fig. 14. MPTS and CHERS contour plots for SN128895: (a) electron temperature, (b) deuterium ion temperature, (c) electron density, (d) toroidal rotation velocity and (e) carbon Z_{eff}.

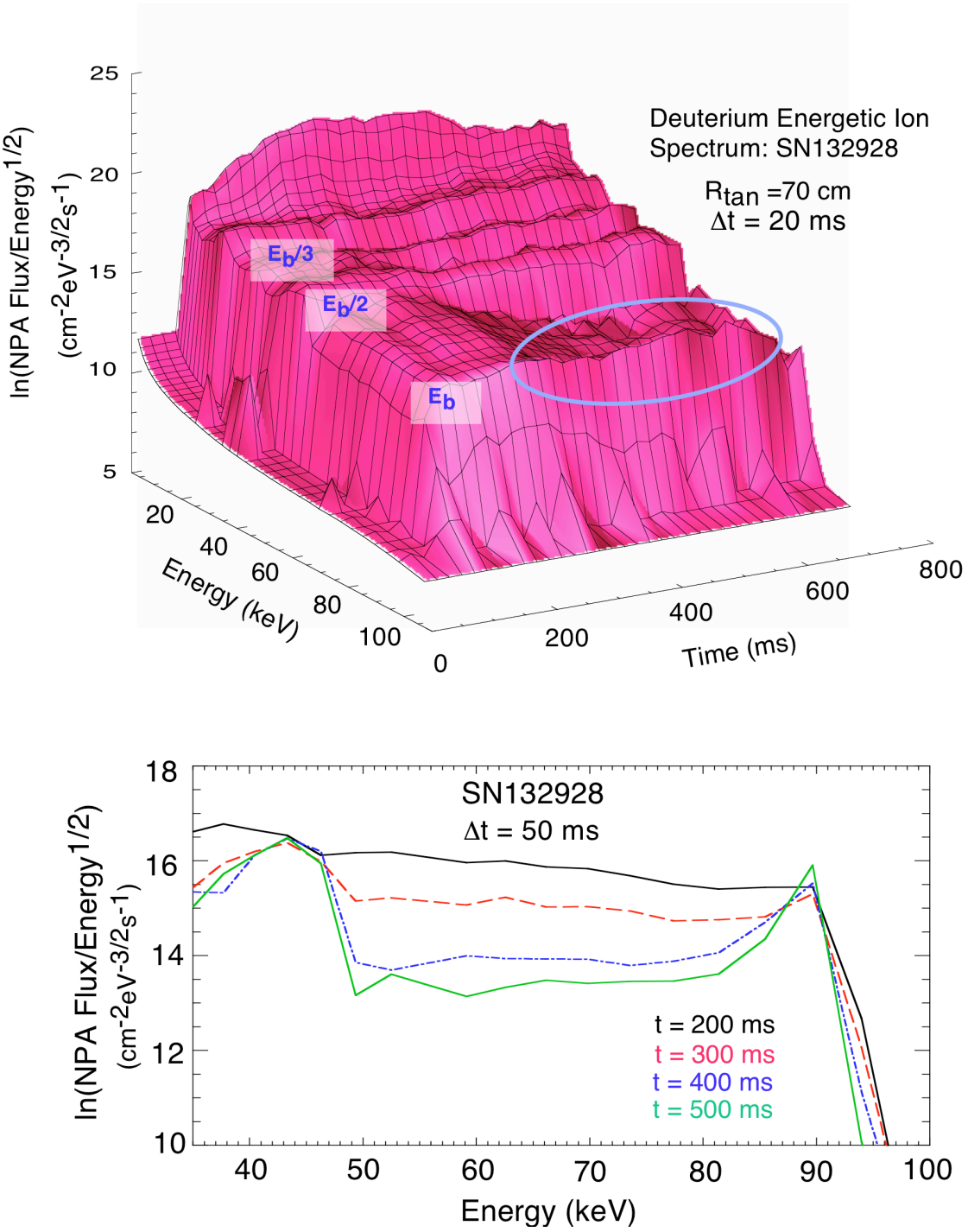

Fig. 15. NPA energetic ion measurements for SN132928 with the NB full, half and third injection energies indicated on the 3D distribution (top) and 2D energy spectrum lineouts at selected times during the discharge (bottom).

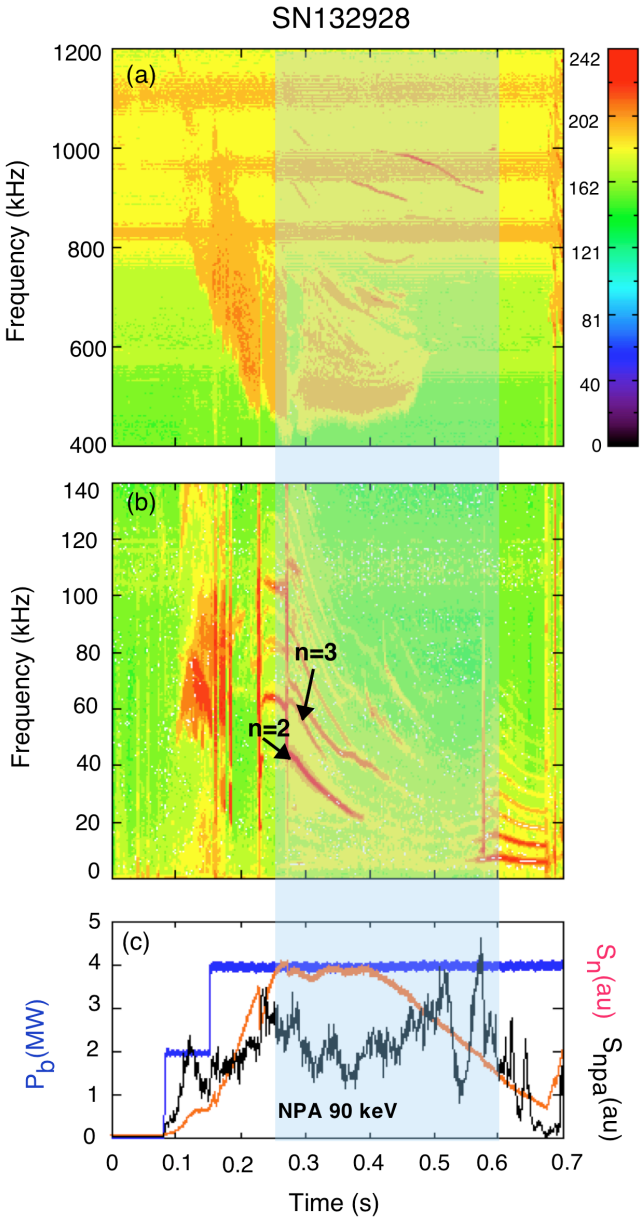

Fig. 16. Mirnov spectrograms for SN132928 in the CAE/GAE (a) and the NTM/TAE (b) regimes plus waveforms showing the injected NB power, NPA signal at E = 90 keV and the volume neutron yield (c).

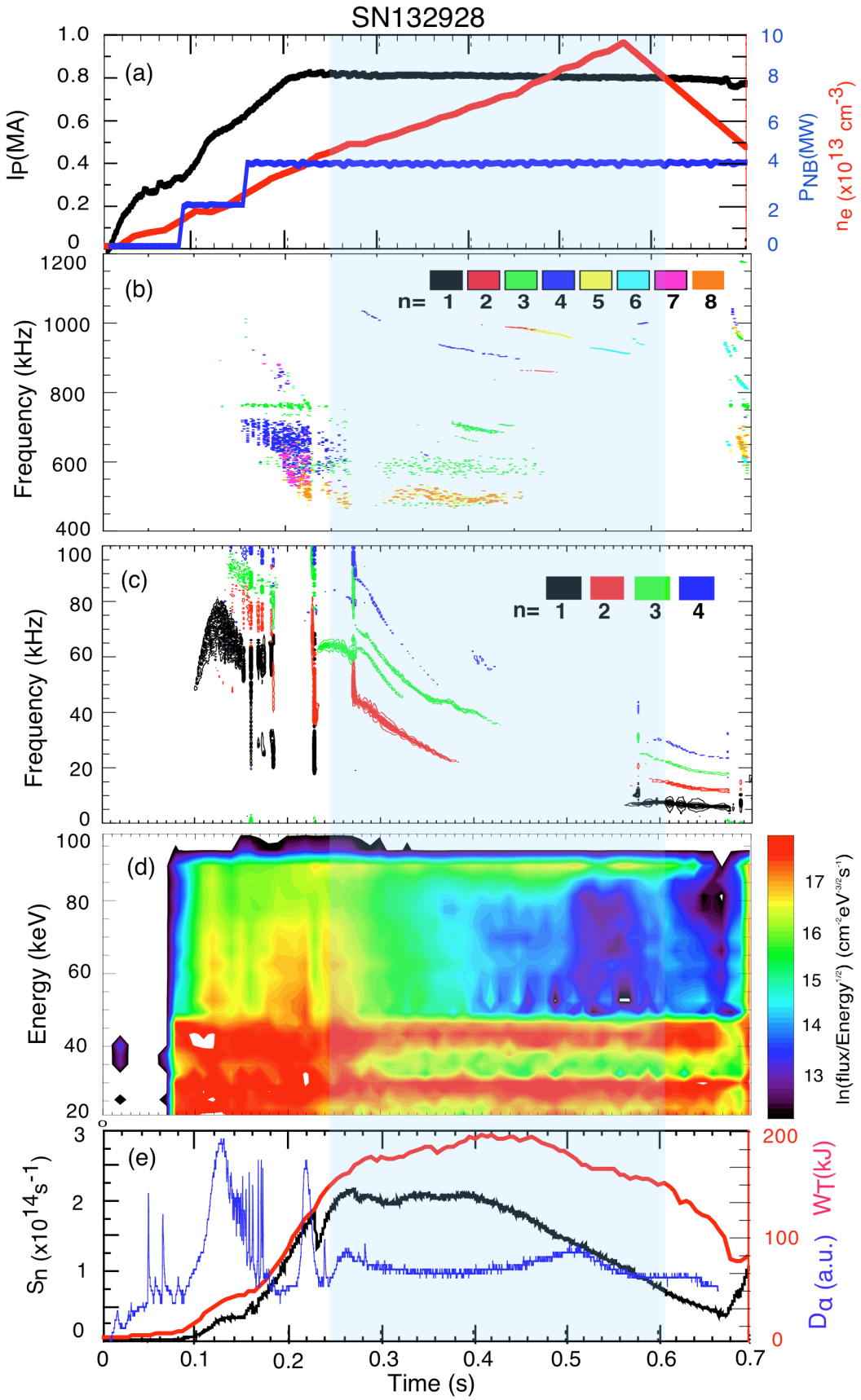

Fig. 17. Selected plasma discharge data for SN132928: (a) plasma current, injected NB power and MPTS line-average electron density, (b) MHD mode analysis for the CAE/GAE regime, (c) MHD mode analysis for the NTM/TAE regime, (d) contour plot of the NPA energetic ion spectrum and (e) volume neutron yield, total stored energy and D_α emission.

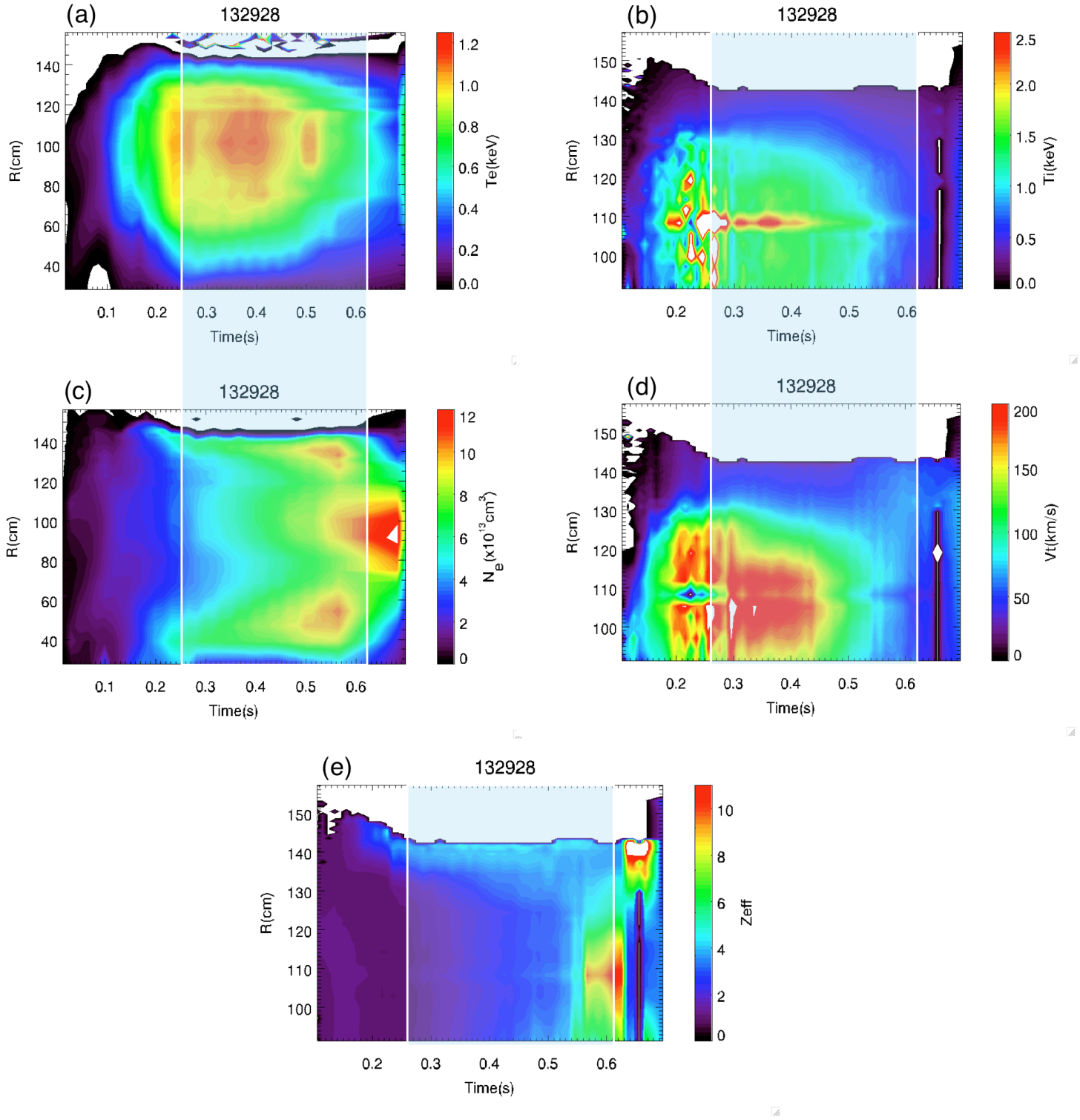

Fig. 18. MPTS and CHERS contour plots for SN132928: (a) electron temperature, (b) deuterium ion temperature, (c) electron density, (d) toroidal rotation velocity and (e) carbon Z_{eff}.

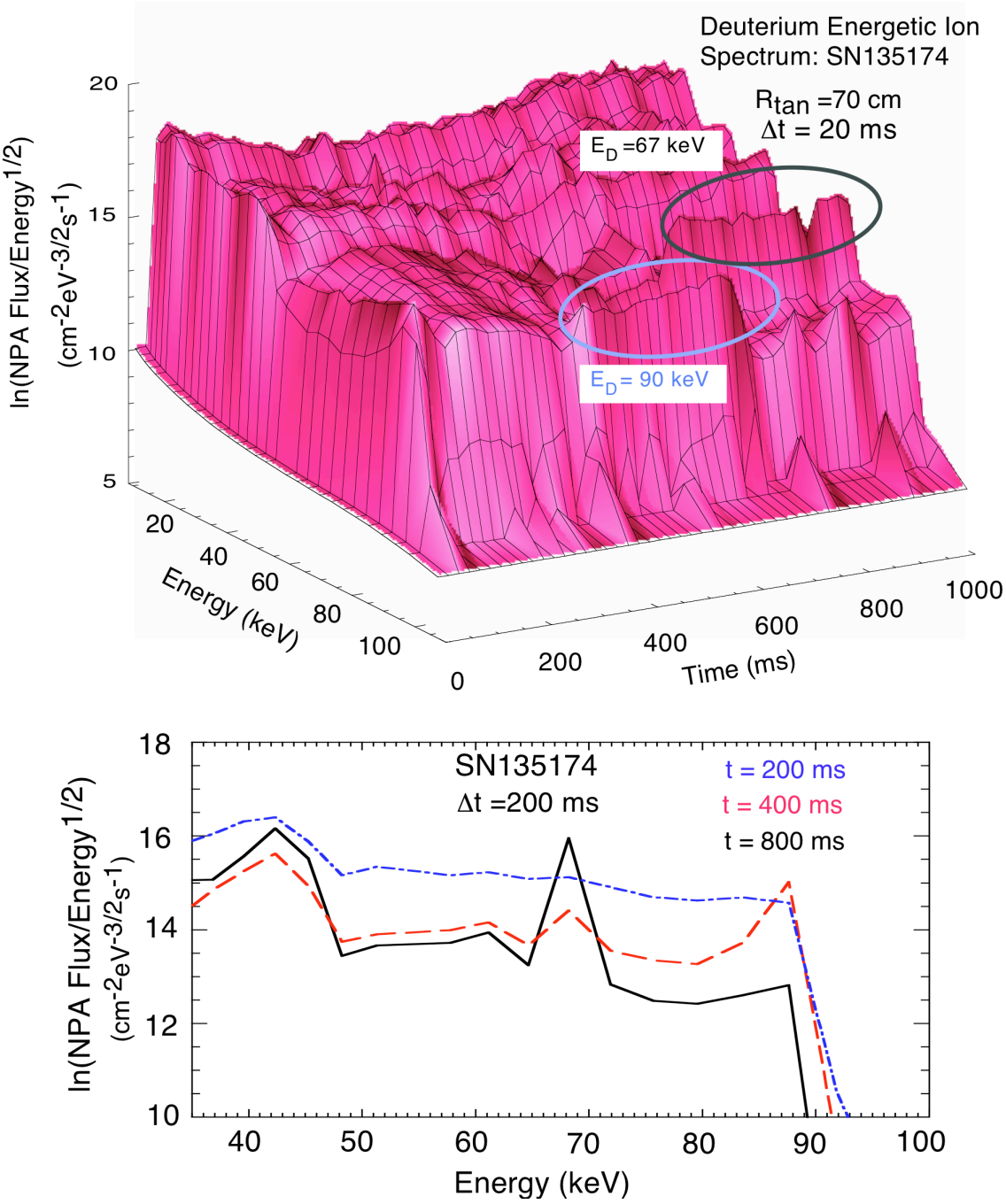

Fig. 19. NPA energetic ion measurements for SN135174 with the NB full, half and third injection energies indicated on the 3D distribution (top) and 2D energy spectrum lineouts at selected times during the discharge (bottom).

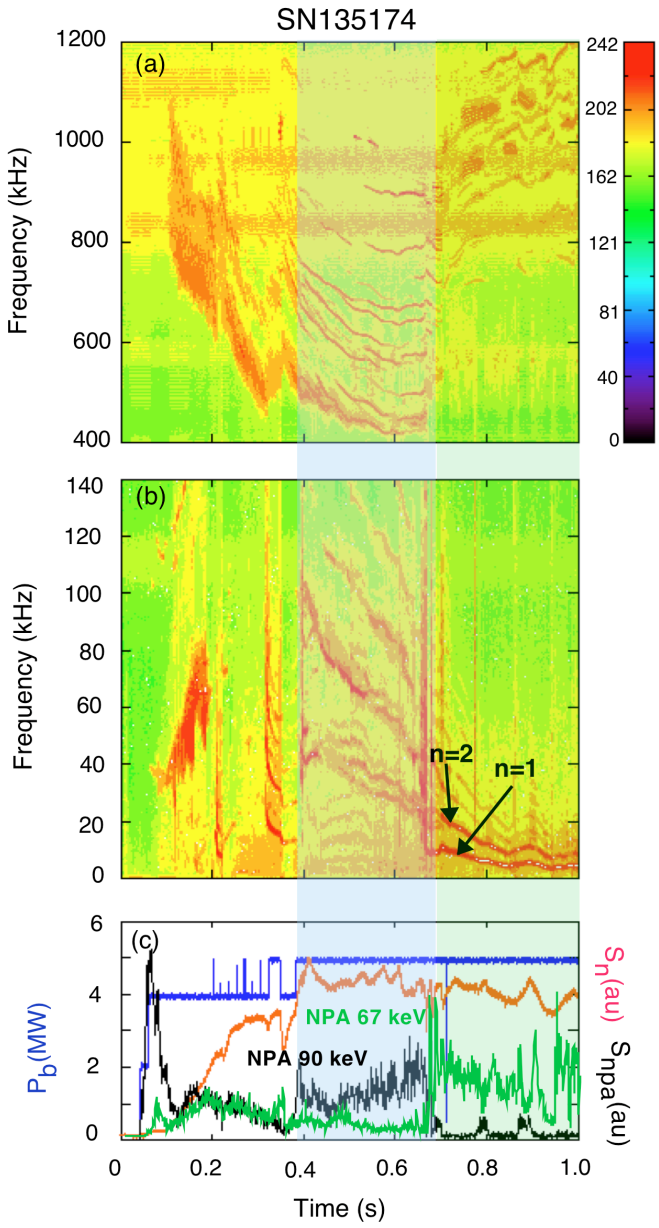

Fig. 20. Mirnov spectrograms for SN135174 in the CAE/GAE (a) and the NTM/TAE (b) regimes plus waveforms showing the injected NB power, NPA signal at E = 90 keV and the volume neutron yield (c).

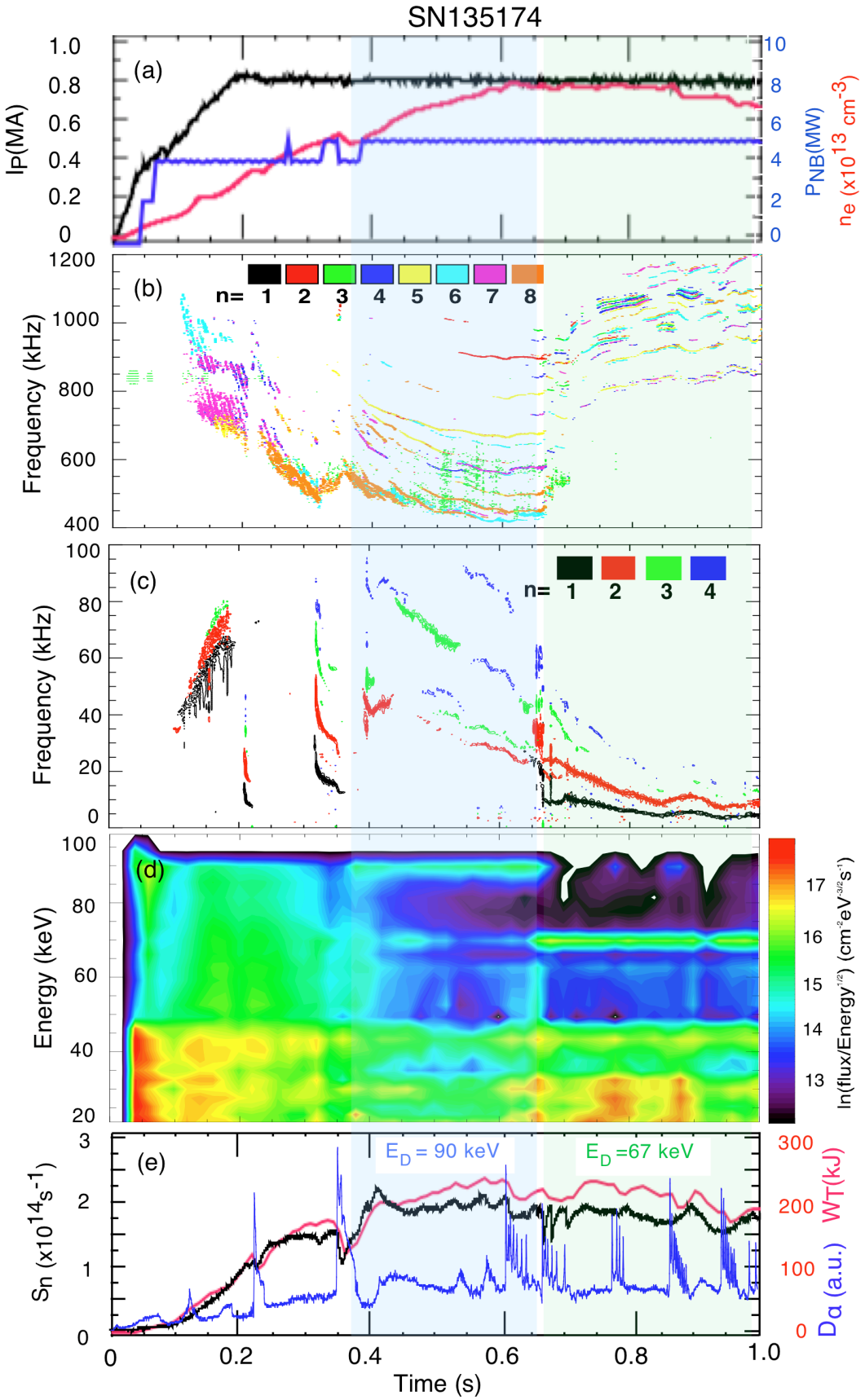

Fig. 21. Selected plasma discharge data for SN1135174: (a) plasma current, injected NB power and MPTS line-average electron density, (b) MHD mode analysis for the CAE/GAE regime, (c) MHD mode analysis for the NTM/TAE regime, (d) contour plot of the NPA energetic ion spectrum and (e) volume neutron yield, total stored energy and D_α emission.

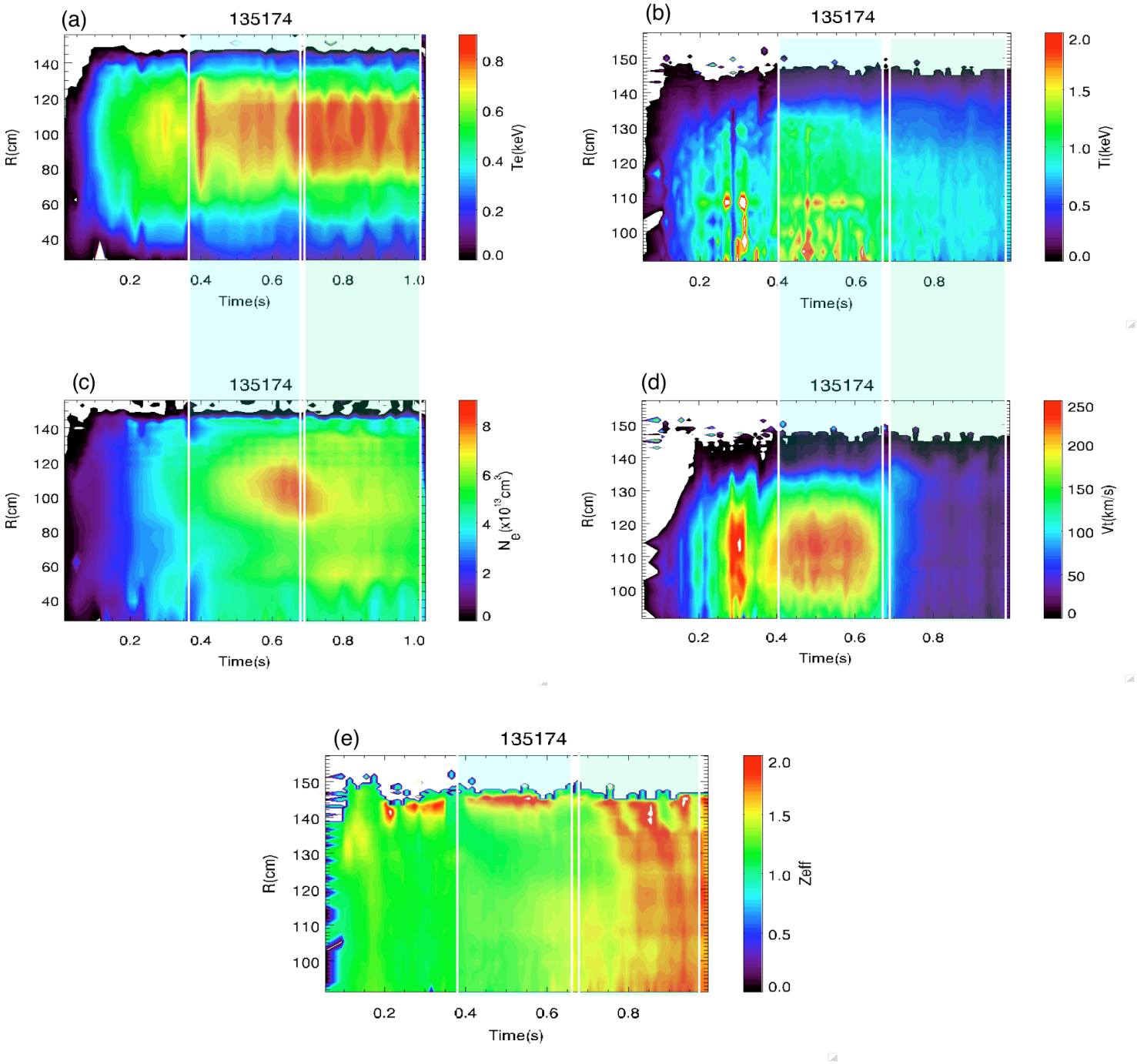

Fig. 22. MPTS and CHERS contour plots for SN135174: (a) electron temperature, (b) deuterium ion temperature, (c) electron density, (d) toroidal rotation velocity and (e) carbon Z_{eff}.

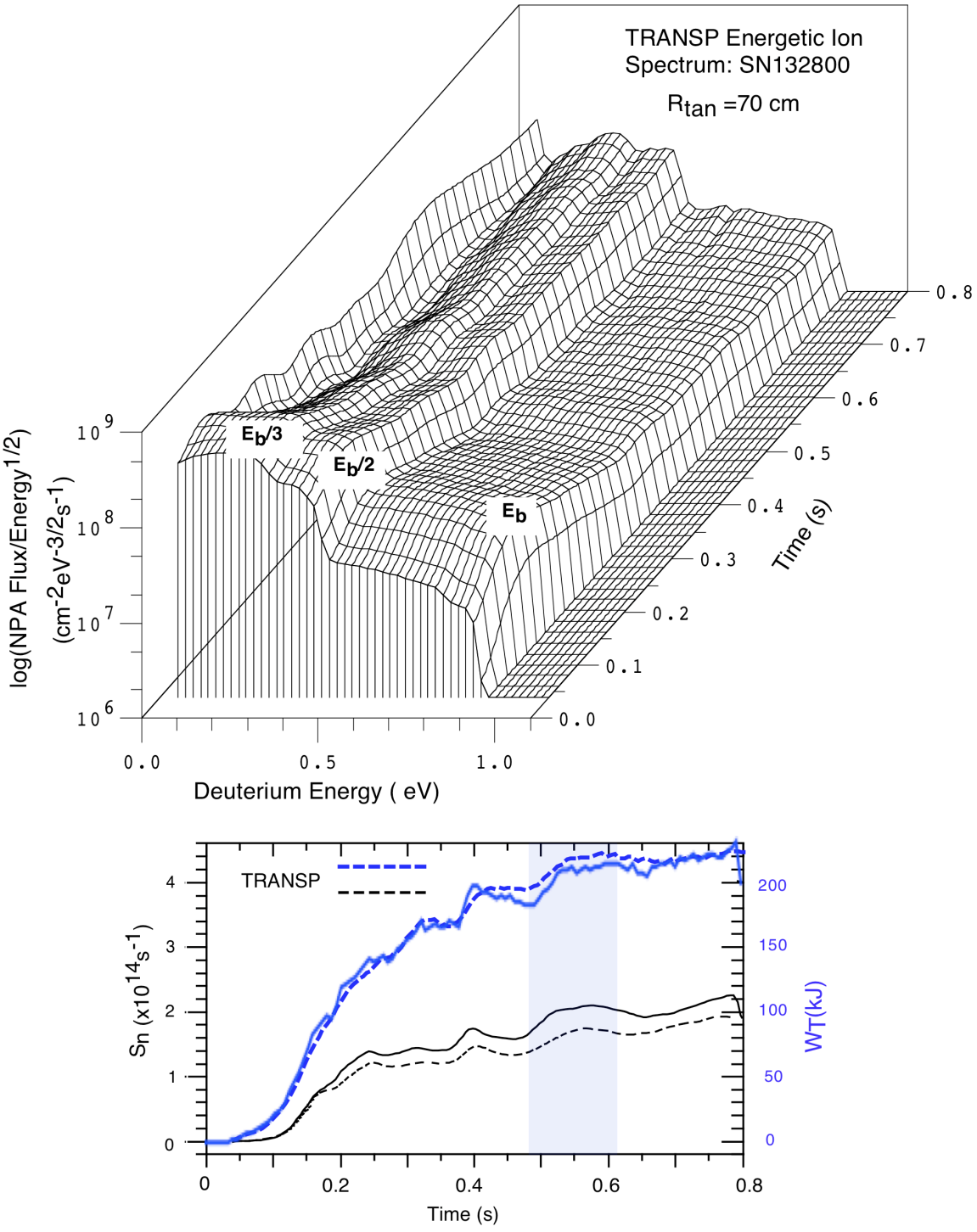

Fig. 23. TRANSP code analysis for SN132800. The TRANSP-simulated NPA energetic ion spectrum (upper plot) is clearly devoid of the HEF observed in the measured spectrum shown in Fig. 7. During the HEF interval demarked by the vertical blue bar, the measured (solid lines) and TRANSP-calculated (dashed lines) time evolution and magnitude of the excursions in S_n and W_T are in good agreement (lower plot).

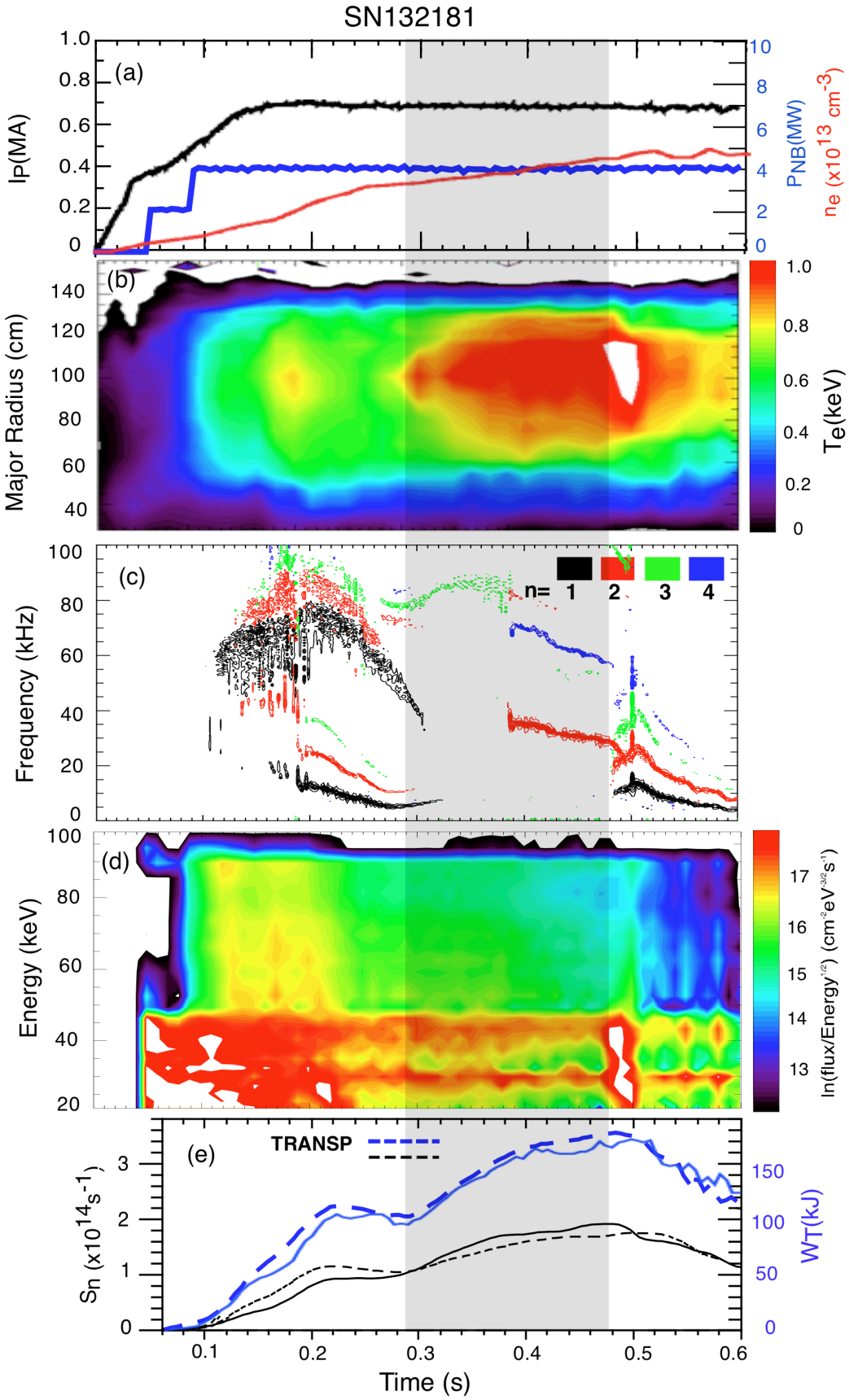

Fig. 24. Selected plasma discharge data for SN132181: (a) plasma current, injected NB power and MPTS line-average n_e, (b) MPTS T_e contour plot, (c) MHD mode analysis for the NTM/TAE regime, (d) contour plot of the NPA energetic ion spectrum and (e) comparison of measured (solid lines) and calclulated (dashed lines) volume neutron yield and total stored energy.

The Princeton Plasma Physics Laboratory is operated
by Princeton University under contract
with the U.S. Department of Energy.

Information Services
Princeton Plasma Physics Laboratory
P.O. Box 451
Princeton, NJ 08543

Phone: 609-243-2245
Fax: 609-243-2751
e-mail: pppl_info@pppl.gov
Internet Address: http://www.pppl.gov